POLITECNICO DI TORINO

Master's Degree
in Electronic Engineering

Master's Degree Thesis

Fine tuning and temperature analysis of capacitive position sensor for shock absorber.

Supervisor
Prof. Marcello Chiaberge
Ing. Gianluca Dara

Candidate
Mattia Dipaola

Academic year 2023-2024

Summary

This thesis work, carried out in collaboration with Marelli Ride Dynamics, focuses on a new non-intrusive position sensor for an active shock absorber based on capacitance measurement. The aim is to take some steps to move from the prototype phase to full-scale production.
The shock absorber is a device used in the automotive field to dampen oscillations by converting kinetic energy mainly into heat.
Knowing precisely the relative position between piston and cylinder in shock absorbers is a very important problem for both comfort and safety reasons. The shock absorber position is in fact used by the anti-lock braking system (ABS) and the electronic stability program (ESP).
Currently the most used position sensor is the HELLA sensor which, due to its anchoring position, is delicate and subject to wear.
The key idea of this innovative new position sensor is to exploit the intrinsic geometry of the shock absorber by using it as a variable capacitor with a capacitance value proportional to the displacement, using the oil in the shock absorber as a dielectric.
To actually make the shock absorber a capacitor it is necessary to change the bushing with an insulated one in order to keep the piston and cylinder electrically insulated.
The developed prototype, realized with the LESS project in 2023, is composed of a circuit for measuring capacitance, consisting of an astable multivibrator that outputs a square wave whose frequency is proportional to the measured capacitance, a microcontroller which uses an interrupt to calculate the input square wave frequency and than translates the value in position and sends it via CAN network. The general scheme of the developed prototype is shown in the following figure.

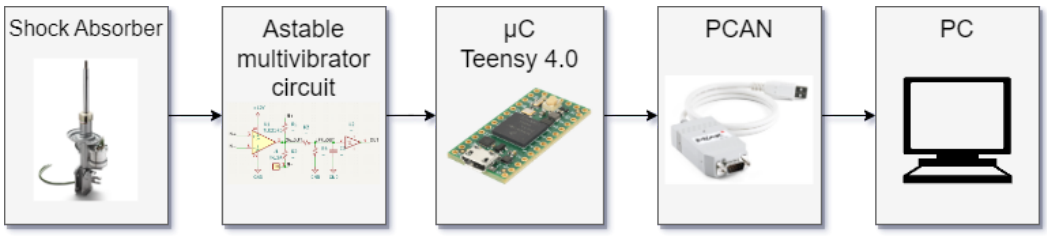

Figure 1. Block diagram of the developed prototype.

Taking into account the non-idealities of the operational amplifier, slew rate and time delay, the frequency-capacitance characteristic follows the experimental values, otherwise the capacitance measurement read by the sensor would be completely wrong.
Initial analyses showed an error of approximately 13 pF between the theoretical characteristic and the experimental values which would result in an error on the displacement of approximately 32 mm.
A first part of this thesis work was to try to reduce the capacitance error read from the sensor by doing a fine calibration of the characteristic by studying the possible sources of parasitic capacitance induced by the connection cables. With the calibration it was possible to obtain a displacement error of approximately 1 mm.
Afterwards, repeatability tests over time and repeatability tests with different prototypes

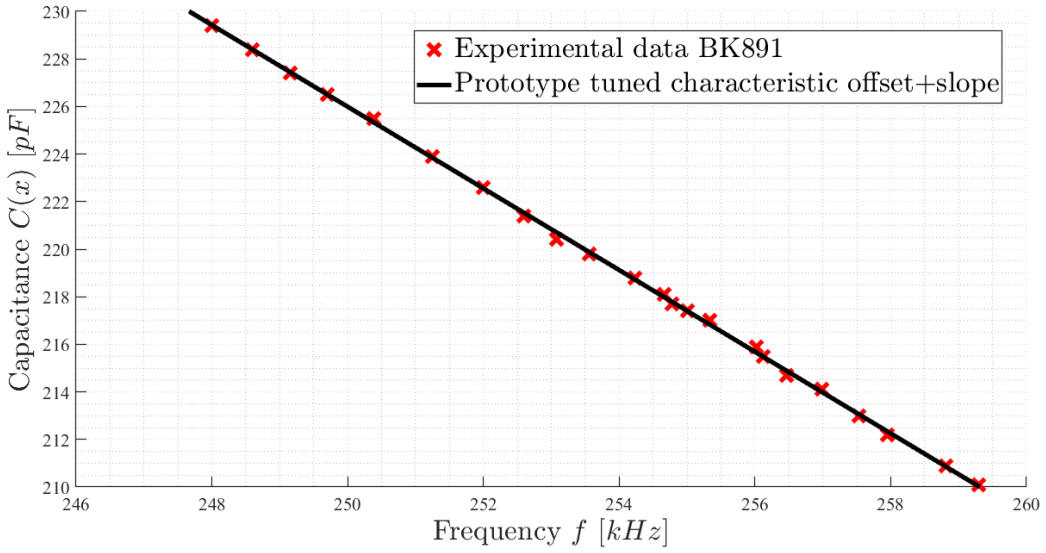

Figure 2. Tuned prototype characteristic with offset and slope correction.

were carried out and differences were observed in the reading attributable to the different temperatures at which the tests were carried out or due to the tolerance of the PCB components.
A calibration state in the microcontroller was therefore proposed in order to perform a calibration based on the different PCBs used.
The variation in dielectric constant of synthetic oil, commonly used in shock absorbers, as the temperature varies was also analyzed in detail.
Through the creation of a test parallel plate capacitor it was possible to measure the dielectric constant-temperature characteristic then used for the correction of the frequency-displacement characteristic as a function of temperature.
The position error without taking into account the variation of dielectric constant with temperature is approximately 4 mm across the entire temperature range.
It was therefore proposed to use a temperature sensor inserted in the PCB in order to

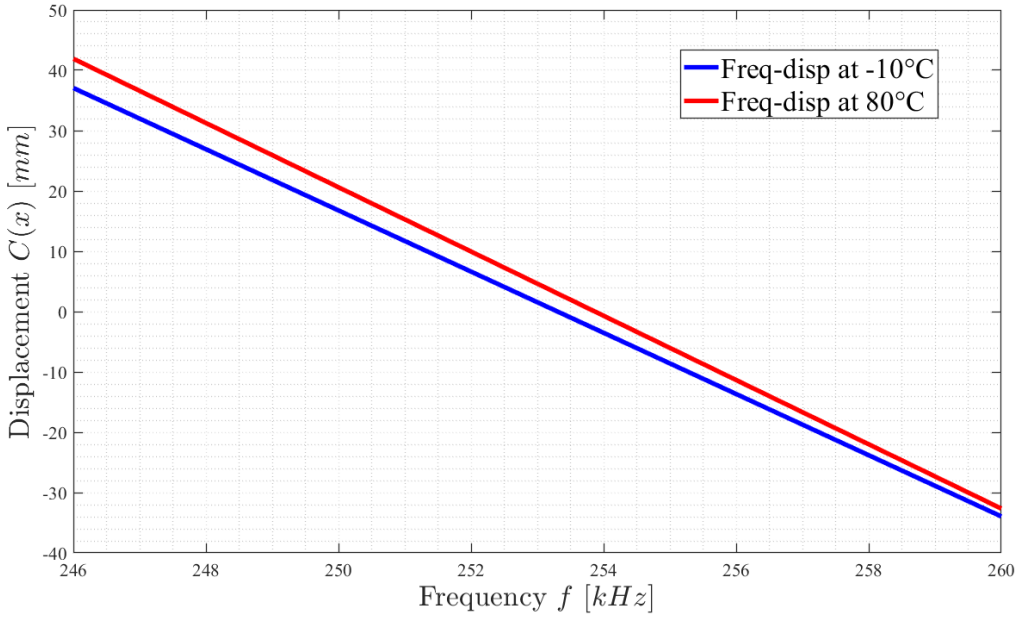

Figure 3. Frequency-displacement characteristics at different temperature.

read the temperature and compensate the characteristic.
Finally, dynamic measurements were carried out using a servo motor controlled in an angular position in order to move a variable capacitor and simulate the trend of the shock absorber.
Datasets of position values of real shock absorbers were used and various digital filters were tested including mean, median on 3 10 and 20 samples and LPF with cut-off frequency of 100 Hz.
The results showed a clear improvement in the measurement and a smaller difference between the position measured by the prototype and the reference position using the mean.
With the use of the 3 and 10 samples median the measured signal is almost as noisy as without the use of filters.
By using the 20 samples median the signal is less noisy but the spikes are attenuated. Therefore, only the use of the mean was chosen.
As a last step, the FFT of the dataset used was carried out to see which frequencies were involved in order to to verify the sampling frequency limit and to reduce the sampling frequency from 100 kHz to 50 Hz using the mean, according to CAN bus communication.

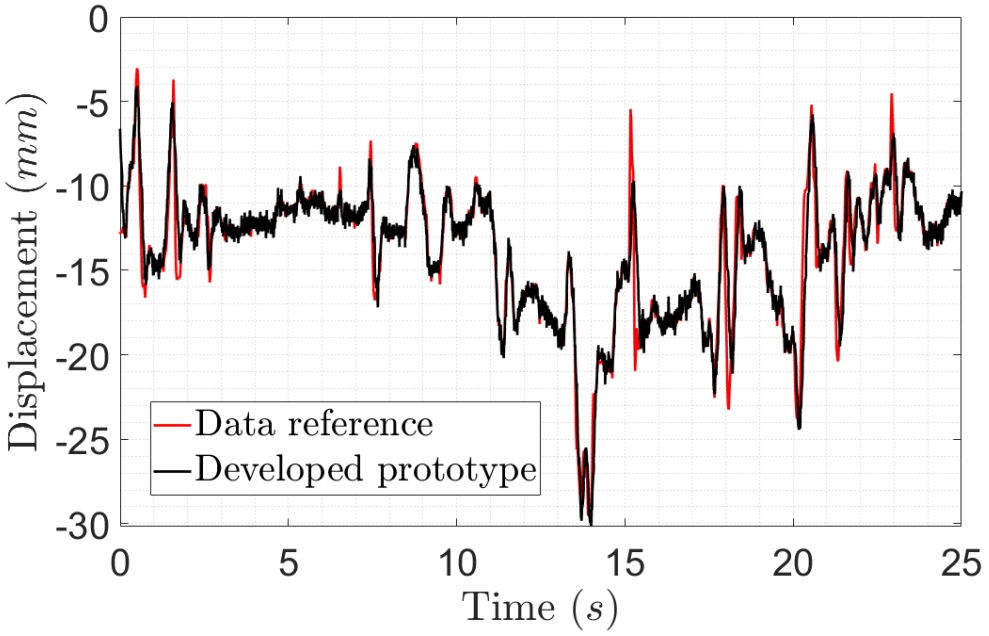

Figure 4. Comparison of dataset #2 and raw measurement of prototype.

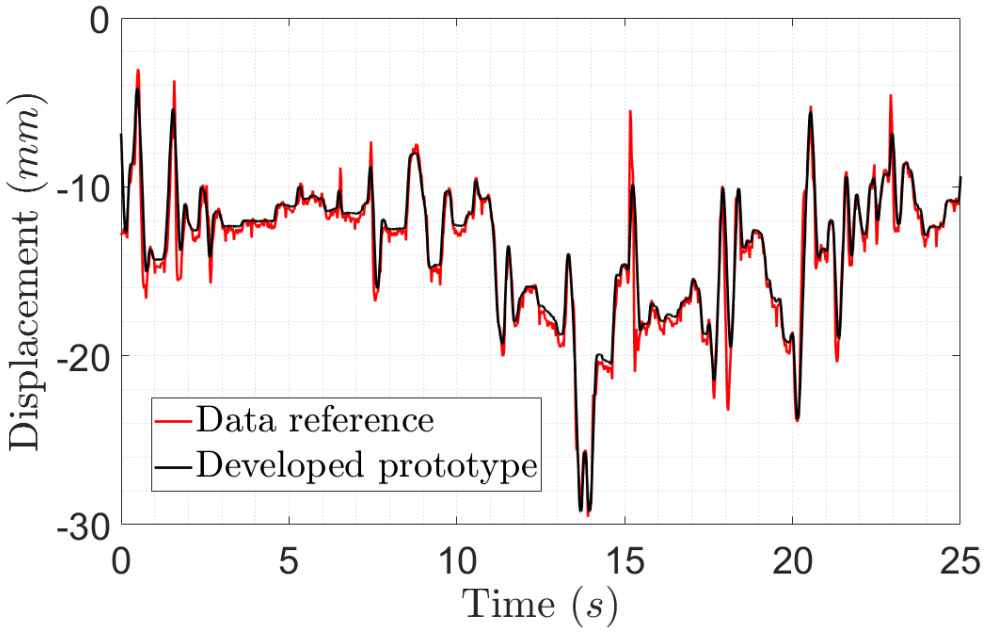

Figure 5. Comparison of dataset #2 and prototype measurement using mean.

Contents

List of Tables

List of Figures

List of Acronyms

AC Alternating Current

CAN Controller Area Network

FFT Fast Fourier Transform

LPF Low Pass Filter

OP-AMP Operational Amplifier

PCB Printed Circuit Board

PWM Pulse-Width Modulation

RMS Root Mean Square

SMD Surface-Mount Device

µC Microcontroller

3D Three Dimensions

Chapter 1

Introduction

This thesis work, carried out in collaboration with Marelli Ride Dynamics, focuses on a new non-intrusive position sensor for an active shock absorber based on capacitance measurement.
In particular, the aim is to first provide a brief overview of the main position sensors currently used in the automotive field, analyzing the critical issues, and then move on to a new innovative non-intrusive position sensor, the development of which has been underway for several years, focusing on the main problems encountered during testing with the aim of making this technology move from the prototype phase to the full-scale production.

1.1 Working principle of shock absorber

The main function of shock absorbers is to dampen the oscillations generated by the suspension by dissipating excess kinetic energy and converting it mainly into heat. As can be seen in figure 1.1, inside the shock absorber, a piston slides inside a cylinder filled with hydraulic oil. When the vehicle hits a bump, the spring compresses, pushing the piston downwards. The hydraulic oil inside the cylinder is forced to pass through small holes that create resistance to movement, slowing the piston and dissipating kinetic energy through friction into heat.
In addition to dampening oscillations, leading to better driving quality. Shock absorbers also serve to stabilize the vehicle and play a fundamental role in safety both during braking and cornering.
Indeed, as mentioned in [ShockAbsorber], without shock absorbers the vehicle's wheels would lose grip due to some deformation of the road surface and could lead to loss of control of the vehicle.

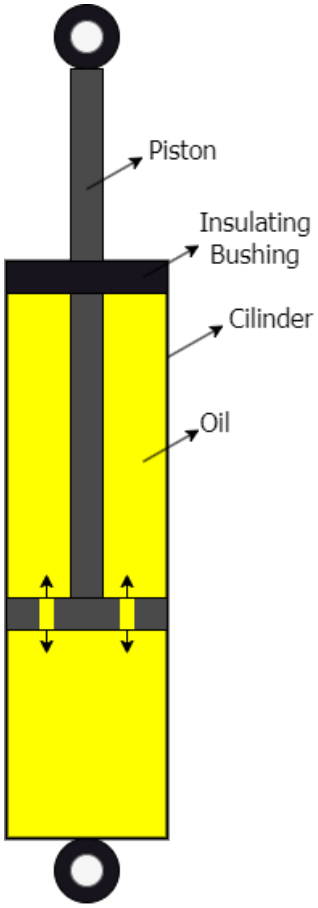

Figure 1.1. General scheme of a shock absorber.

Shock absorbers are mainly divided into active, passive and semi-active. Differentiated not only by their internal structure but also by the functions they are able to perform.

- **Passive shock absorber**
  Passive shock absorbers have fixed damping which depends on the viscosity of the oil used, in these shock absorbers it is not possible to act to modify this damping value.
- **Semi-active shock absorber**
  Semi-active shock absorbers, on the other hand, can vary the damping value by acting on the alteration of the oil flow by partially closing a valve.
  The most common method to change the flow is by using a solenoid valve, injecting current into a solenoid.

They are called semi-active because they do not add energy to the system, essentially not applying an opposing force to the movement of the suspension.

- **Active shock absorber**
  Contrary to semi-active shock absorbers, active shock absorbers use actuators to apply a force independent of the suspension, these actuators are generally electric motors.
  In this type of shock absorbers, electromagnetic motors can also be used as generators in order to recover and convert part of the kinetic energy into electricity.
  Active shock absorbers are able to guarantee better vehicle handling and better driving quality but are generally very complex and high cost.

1.2 Position sensor motivation

Having precise knowledge of the position of the piston relative to the cylinder in real time is very important for several reasons.
First of all this value is used for control systems that affect the safety of the vehicle such as the anti-lock braking system (ABS) or the electronic stability program (ESP).
In addition, it can be very important in vehicles with semi-active or active shock absorbers to set the best configuration depending on the type of terrain you are traveling on.
The position of the shock absorber is also useful in new technologies such as in adaptive headlights in which during cornering the headlights illuminates the road in the direction of the turn.

1.3 Overview of main position sensors

In the following section lists the main position sensors currently used in the automotive sector [ActiveSensors].
The aim is to give a general overview of the operating principles of each sensor to understand and analyze its critical issues.

- **Linear and angular potentiometer**
  Linear potentiometer sensors are made up of a resistive string and a slider on the piston that creates contact by modifying the resistance.

Based on the measured resistance, the displacement can be estimated. These types of sensors can be mounted inside or outside the cylinder, however they complicate the design and are subject to wear.
There is also the analogous angular version in which the resistivity variation is directly linked to the angular variation.

Figure 1.2. Linear potentiometer sensor.

- **Induction sensor**
  In inductive sensors we have an external coil that wraps the cylinder whose inductance is modified by the piston which is made of ferromagnetic material. Generating a variation in inductance proportional to the displacement of the piston.
  The main drawbacks of this sensor are the high cost to make the coil and the constrain in using ferromagnetic materials for the piston.
  Another critical issue of this sensor is the excitation frequency of the current in the coil which determines both the sensitivity and precision of the measurement but also the dynamic range of the sensor. However, they are less invasive than potentiometric sensors.

- **HELLA inductive sensor**
  Another type of induction sensor is the one developed by HELLA as can be read in [HellaSensor].
  This sensor is the most widespread in the automotive sector both for measuring the position of the shock absorber but is also used to measure the position of the accelerator pedal or the steering angle.
  The HELLA sensor is an angular sensor therefore the inductance varies depending

on the angle, the position as a function of the inductance is calculated through an ASIC (application specific integrated circuit).

The main disadvantage of this sensor is its fragility, resulting from the position in which it is installed. The sensor is mounted near the shock absorber, therefore external to the shock absorber itself.
However, constant exposure to environmental conditions such as water and mud and mechanical stress makes the sensor vulnerable to damage and wear.

Figure 1.3. Hella inductive sensor.

- **Magnetic hall sensor**
  Hall effect magnetic sensors are based on the measurement of magnetic fields without any contact. The sensor involves the use of permanent magnets and a strip of hall-effect sensors on the cylinder. Hall effect sensors measure the magnetic field which is proportional to the displacement of the shock absorber.
  This design is also intrusive to the shock absorber design and subject to wear.

- **Linear Variable Differential Transformer**
  LVDT sensors are among the most complex position sensors, composed of a primary coil on the cylinder followed by two secondary coils. The piston is made of ferromagnetic material and moves freely inside the cylinder without being in contact with the coils.
  The primary coil is powered with AC current at a certain frequency, due to the ferromagnetic material piston, a voltage is generated on the secondary coil proportional to the displacement.

This sensor is highly intrusive and completely changes the design of the shock absorber, making the structure much more complicated.
Being a sensor that measures a magnetic field must be appropriately shielded to avoid disturbances coming from the environment.

Figure 1.4. LVDT sensors.

1.4 Non intrusive capacitive position sensor

The key idea behind this new capacitive sensor is to exploit the structure of the shock absorber itself, composed of piston and cylinder, in order to make it a variable capacitor whose capacitance value varies as the position varies.
This measurement method is considered non-intrusive because it only requires access to the piston and cylinder in order to calculate the displacement without changing the scructure of the shock absorber.

Chapter 2

Capacitance model of shock absorber

2.1 Shock Absorber design

To actually make the shock absorber a capacitor it is necessary to isolate the piston and cylinder.
In a normal shock absorber, since the bushing is made of ferromagnetic material, the piston and cylinder are short-circuited.
To electrically isolate the piston and cylinder, simply replace the bushing with an insulated one.
With this modification the shock absorber is in effect a capacitor whose dielectric material is the internal oil.

2.2 Mathematical modeling of displacement-capacitance characteristic

Due to the changes mentioned above, the intrinsic geometry of the shock absorber is effectively a variable capacitor whose capacitance varies depending on the position since it is two conductive surfaces with a dielectric in between. The total capacitance can be divided into several sources of capacitance, some with parallel plate (2.1) and others cylindrical (2.2).

$$C = \frac{\epsilon_r \epsilon_0 A}{x} \tag{2.1}$$

$$C = \frac{2\pi \epsilon_r \epsilon_0 x}{ln(\frac{r2}{r1})} \tag{2.2}$$

Where the ϵ_r is the dielectric constant of dielectric material, A is the area and x is the distance between the two armature.
All possible sources of capacitance in a generic shock absorber are shown in the figure 2.1.

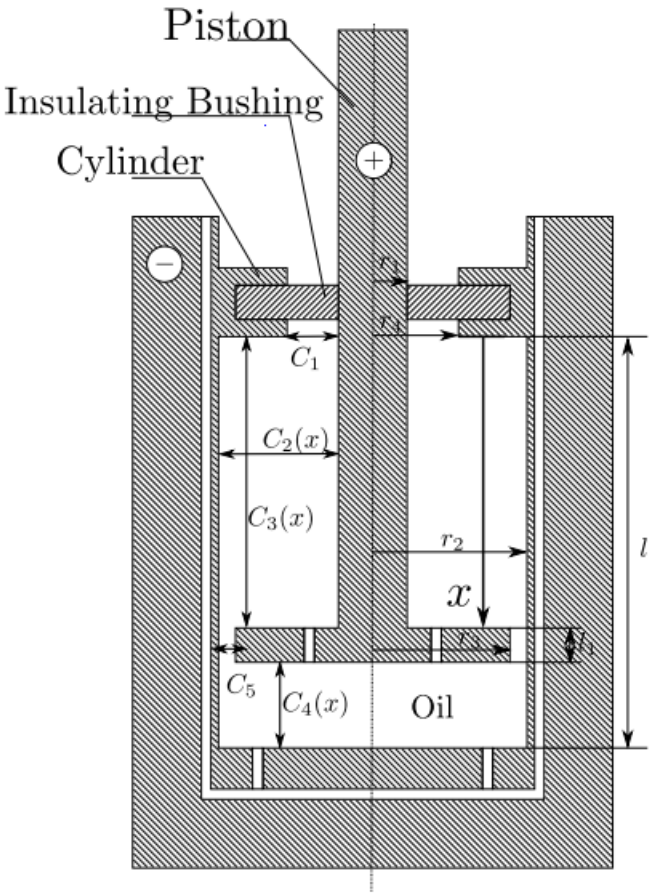

Figure 2.1. Capacitance model of a generic shock absorber.

Some capacities are fixed, such as C_1 and C_5 , others vary as position x varies such as $C_2(x)$, $C_3(x)$ and $C_4(x)$. The total capacitance is given by (2.3).

$$C(x) = C_1 + C_5 + C_2(x) + C_3(x) + C_4(x) \tag{2.3}$$

Using the correct formula for all the capacitance we obtain (2.4) that describe the relation between the total capacitance of the shock absorber with the displacement x.

$$C(x) = C_0 + \frac{2\pi\epsilon_{oil}\epsilon_0 x}{ln(\frac{r_2}{r_1})} + \frac{\pi\epsilon_{oil}\epsilon_0(r_3)^2}{l - x - l_1} + \frac{\pi\epsilon_{oil}\epsilon_0(r_3 - r_4)^2}{x} \tag{2.4}$$

The fixed capacitance $C_0 = C_1 + C_5$ can be experimentally computed measuring the capacitance of the shock absorber in full extension and just adds an offset at the total capacitance.
The figure 2.2 show the relation between the capacitance and the displacement of (2.4) with given mechanical dimensions: $r_1 = 22$ mm, $r_2 = 32$ mm, $r_3 = 31.5$ mm, $r_4 = 24$ mm, $l = 160$ mm, $l_1 = 10$ mm; the dielectric constant of the oil $\epsilon_{oil} = 2.13$; the point x = 0 show the value of $C_0 \approx 200$ pF.
The relationship between capacitance and displacement is non-linear and the main contribution of the total capacitance is given by the cylindrical capacitance $C_2(x)$ so the (2.4) can be simplified as (2.5).

$$C(x) \approx C_0 + \frac{2\pi\epsilon_{oil}\epsilon_0 x}{ln(\frac{r_2}{r_1})} \tag{2.5}$$

The derivative of (2.5) shows the precision of the displacement measurement as a function of the precision of the the capacitance (2.6). For instance to have a precision of ± 1 mm in the displacement require a ±0.4 pF of precision in the measurement of capacitance.

$$\Delta C = \frac{2\pi\epsilon_{oil}\epsilon_0}{ln(\frac{r_2}{r_1})}\Delta x \tag{2.6}$$

Since the capacitance values of the shock absorber are in the order of 200 pF and the sensitivity of the capacitance-displacement characteristic is 0.4 pF/mm, it is necessary to keep under control any sources of parasitic capacitance that could vary the capacitance value of the shock absorber. High precision in capacitance measurement is also necessary in order to have high precision in position measurement.

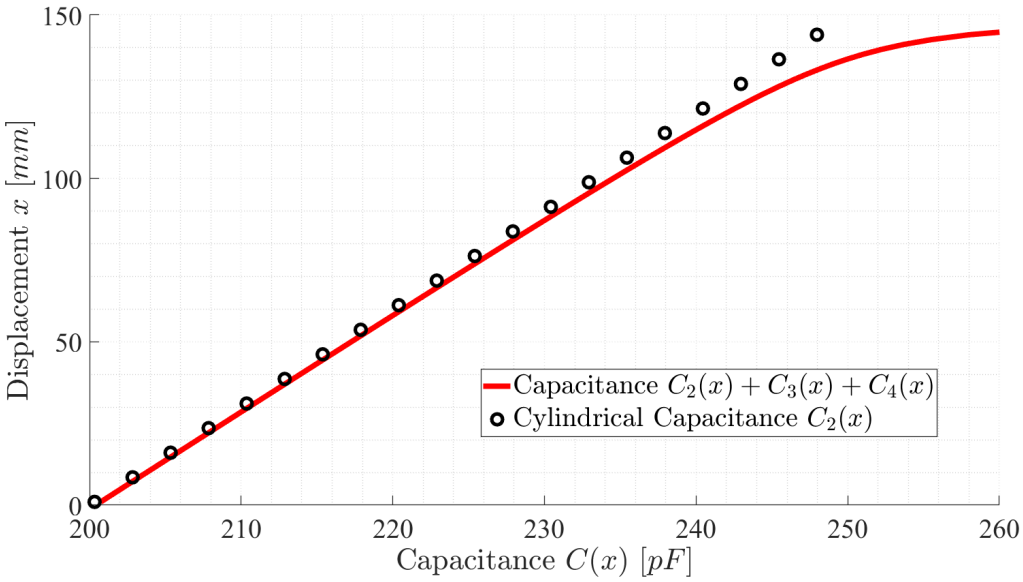

Figure 2.2. Capacitance-displacement characteristic.

Chapter 3

Developed prototype and state of art

The working principles of the developed prototype is shown in figure 3.1. In particular the shock absorber is directly connected to an astable multivibrator circuit that have a proper threshold in order to generate a square wave with frequency proportional to the capacitance of the shock absorber, the frequency of the output square wave is measured with a microcontroller and then converted to position via a linear frequency-position law. After that the correct value of position will be sent through a CAN and displayed on the PC by a PCAN-USB adapter.
The prototype of the capacitive position sensor for shock absorber was previously developed and physically realized with the LESS project and all the design details are reported in the article [Marcello Chiaberge [19-21 July 2023]].

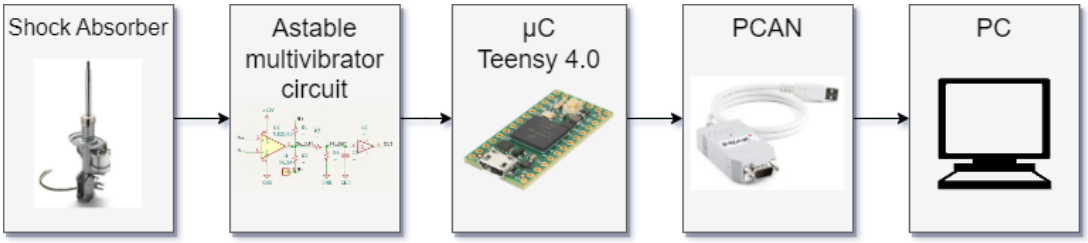

Figure 3.1. Block diagram of the developed prototype.

3.1 Astable multivibrator circuit

The astable multivibrator circuit is an square-wave generator where the frequency of the square-wave depends on the capacitance connected in the inverting port.
The astable multivibrator circuit was chosen over others for its simplicity, in fact it does not require switches or any external waveform generator and has a single supply feature which makes it compatible with the automotive environment where only a single power supply is present.
In this way is possible to create a cheaper and smaller sensor for automotive application.
The astable multivibrator circuit used in the prototype is shown in figure 3.2.
The operational amplifier compare the voltages across its two input and gives the output that can be positive or negative depending on the voltage of capacitor and the thresholds.
In this circuit the operational amplifier works in saturation mode, so the only two output voltages can be V_{sat}^{+} and V_{sat}^{-}.
The constant voltage V_{in} is used to produce a asymmetric thresholds in order to use the operational amplifier with a single-supply voltage.

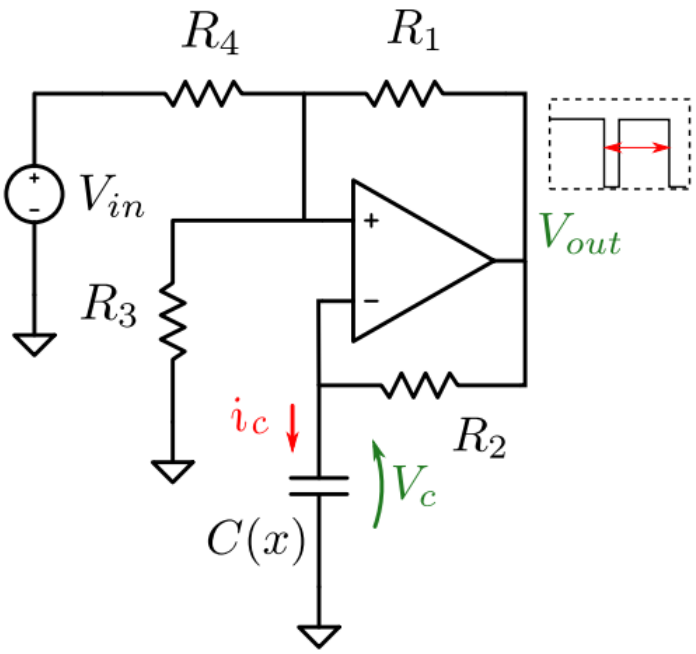

Figure 3.2. Single supply astable multivibrator circuit.

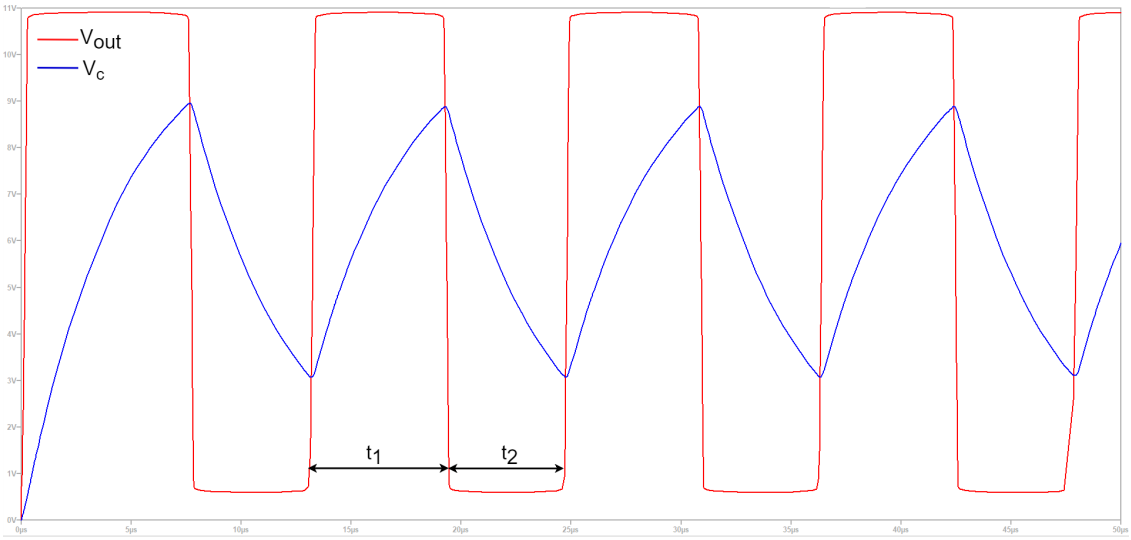

Figure 3.3. SPICE simulation of astable multivibrator with TLE2142.

Let's suppose that the capacitor is fully disharged and at t=0 starts to charge with time constant $\tau = RC$.
The voltage across the capacitor C(x) can be written as 3.1 where the time constant $\tau = RC$.

$$V_c(t) = V_c(\infty) + [V_c(0) - V_c(\infty)]e^{-\frac{t}{\tau}} \tag{3.1}$$

At time $t = t_1$, as shown in 3.2, the voltage across the capacitor reach the V_{th}^+ and the capacitor starts to discharge due to switching the op-amp output to V_{sat}^-.
At time $t = t_2$, as shown in 3.3, after the voltage across the capacitor reaches the V_{th}^- the op-amp switches its state again.

$$V_c(t_1) = V_{th}^+ = V_{sat}^+ + [V_{th}^- - V_{sat}^+]e^{-\frac{t_1}{R_2C}} \tag{3.2}$$

$$V_c(t_2) = V_{th}^- = V_{sat}^- + [V_{th}^+ - V_{sat}^-]e^{-\frac{t_2}{R_2C}} \tag{3.3}$$

Where the V_{th}^+ and V_{th}^- are evaluated by (3.4) and (3.5).

$$V_{th}^+ = V_{in}\left(\frac{R_1||R_3}{R_4 + R_1||R_3}\right) + V_{sat}^+\left(\frac{R_4||R_3}{R_1 + R_4||R_3}\right) \tag{3.4}$$

$$V_{th}^{-} = V_{in}\left(\frac{R_1||R_3}{R_4 + R_1||R_3}\right) + V_{sat}^{-}\left(\frac{R_4||R_3}{R_1 + R_4||R_3}\right) \tag{3.5}$$

From these two formulas we can then calculate the charging time t_1 (3.6) and the discharge time t_2 (3.7) which will correspond to the period of the output square wave.

$$t_1 = R_2 C(x) ln\left(\frac{V_{th}^{-} - V_{sat}^{+}}{V_{th}^{+} - V_{sat}^{+}}\right) \tag{3.6}$$

$$t_2 = R_2 C(x) ln\left(\frac{V_{th}^{+} - V_{sat}^{-}}{V_{th}^{-} - V_{sat}^{-}}\right) \tag{3.7}$$

So the oscillation frequency will be (3.8).

$$f(x) = \frac{1}{t_1 + t_2} \tag{3.8}$$

Substituting formulas (3.6) and (3.7) into (3.8) we obtain the formula for the capacitance as a function of x.
As we can see from (3.9) the capacitance value depends only on the resistance R2, the output oscillation frequency, the op-amp saturation values and the set threshold values.

$$C(x) = \frac{1}{R_2 \cdot f \cdot ln\left(\frac{V_{th}^{+} - V_{sat}^{-}}{V_{th}^{-} - V_{sat}^{-}} \frac{V_{th}^{-} - V_{sat}^{+}}{V_{th}^{+} - V_{sat}^{+}}\right)} \tag{3.9}$$

It is therefore possible to calculate the capacitance value simply by reading the frequency value of the output square wave due to all the other variables are known having been chosen in the design phase.

3.1.1 Non-idealities of the astable multivibrator

In order to not overestimate the oscillation frequency, non-idealities must be considered. First of all, the capacitor C(x) is not charged with a fixed voltage equal to Vh due to the slew rate of the op-amp, as happens during the discharge phase.
As we can see in figure 3.4 the capacitor undergoes an overshoot, as long as the output voltage is less than the capacitor voltage the capacitor continues to charge.
The equation that describes the behavior of the voltage on the capacitor is the differential equation (3.10) which has the solution (3.11), where s_r is the slew rate of the op-amp and

λ is (3.12).

$$\frac{dV_c}{dt} = \frac{1}{R_2 C(x)}(s_r t - V_c) \tag{3.10}$$

$$V_c(\lambda) = e^{-\lambda}(V_c(t_0) + s_r R_2 C(x)(e^{\lambda}(\lambda - 1) + 1)) \tag{3.11}$$

$$\lambda = \frac{t}{R_2 C(x)} \tag{3.12}$$

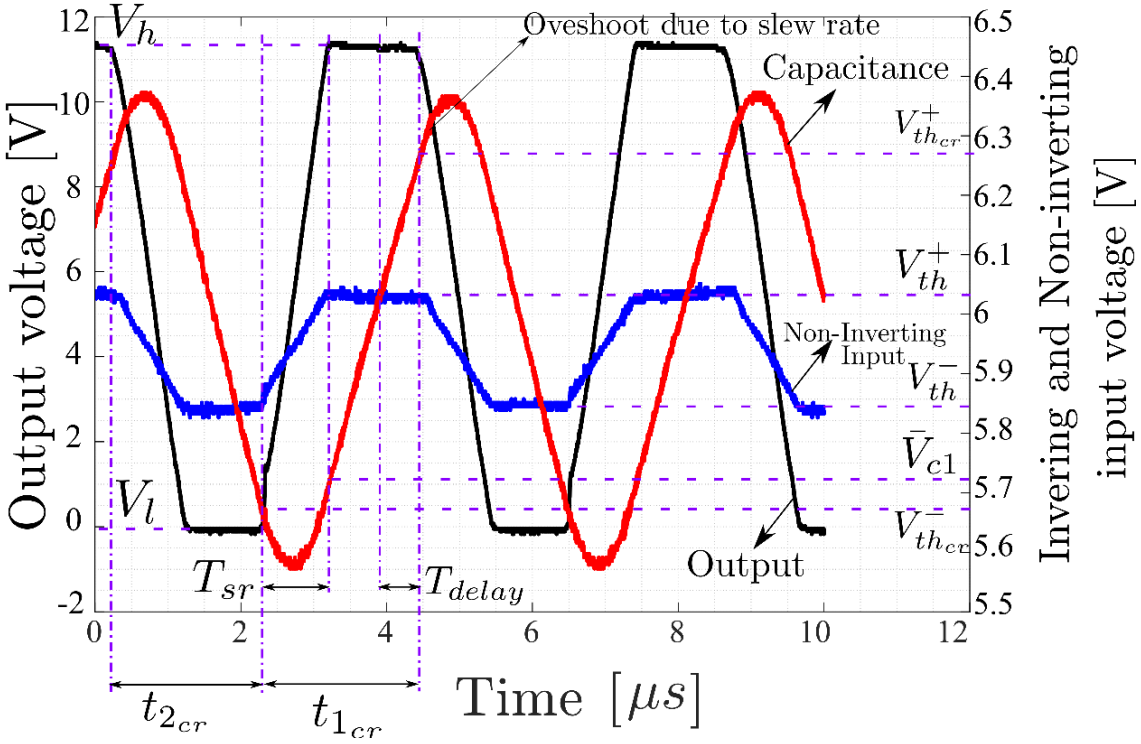

Figure 3.4. Measured voltages on the non-inverting port, inverting port, and output of the oscillator stage with C(x) = 255 pF.

In addition to this there is a T_{delay} between when the capacitor voltage exceeds the voltage value of the non-inverting gate and between when the op-amp starts to change its output from V_{sat}^+ to V_{sat}^- and vice versa as shown in figure 3.4.
This delay is due to the time required to charge the op-amp's parasitic capacitances.
To compensate for this error, new threshold values must be used as shown in (3.13) and

(3.14).

$$V_{th_{cr}}^{+}(C(x)) = V_{th}^{+} + T_{delay} \left.\frac{dV_c}{dt}\right|_{t=0, V_c(0) \approx V_{th}^{-}} \tag{3.13}$$

$$V_{th_{cr}}^{-}(C(x)) = V_{th}^{-} - T_{delay} \left.\frac{dV_c}{dt}\right|_{t=0, V_c(0) \approx V_{th}^{+}} \tag{3.14}$$

Differential equation (3.10) is then used to calculate the capacitor voltage taking into account the non-linearities of overshoot, delay and slew rate of the op-amp.
In particular (3.11) is used with $\lambda = \frac{T_{slew}}{R_2 C(x)}$ and $V_c(t_0)$ is equal to $V_{th_{cr}}^{-}$ or $V_{th_{cr}}^{+}$ respectively as shown in (3.16) and (3.17), where T_{sr} is equal to (3.15).

$$T_{sr} = \frac{V_{sat}^{+} - V_{sat}^{-}}{s_r} \tag{3.15}$$

$$\overline{V}_{c1}(x) = e^{-\frac{T_{slew}}{R_2 C(x)}} \left(V_{th_{cr}}^{-} + s_r R_2 C(x) \left(e^{\frac{T_{slew}}{R_2 C(x)}} \left(\frac{T_{slew}}{R_2 C(x)} - 1 \right) + 1 \right) \right) \tag{3.16}$$

$$\overline{V}_{c2}(x) = e^{-\frac{T_{slew}}{R_2 C(x)}} \left(V_{th_{cr}}^{+} + s_r R_2 C(x) \left(e^{\frac{T_{slew}}{R_2 C(x)}} \left(\frac{T_{slew}}{R_2 C(x)} - 1 \right) + 1 \right) \right) \tag{3.17}$$

The new corrected $t_{1_{cr}}$ and $t_{2_{cr}}$ are then obtained using the new previously calculated capacitor voltages as shown in (3.18) and (3.19).

$$t_{1_{cr}}(x) = R_2 C(x) ln \left(\frac{\overline{V}_{c1}(C(x)) - V_{sat}^{+}}{V_{th_{cr}}^{+}(C(x)) - V_{sat}^{+}} \right) + T_{sr} \tag{3.18}$$

$$t_{2_{cr}}(x) = R_2 C(x) ln \left(\frac{\overline{V}_{c2}(C(x)) - V_{sat}^{-}}{V_{th_{cr}}^{-}(C(x)) - V_{sat}^{-}} \right) + T_{sr} \tag{3.19}$$

The final formula that links the oscillation frequency of the output square wave to the change in capacitance of the capacitor is therefore given by (3.20).

$$f_{cr}(x) = \frac{1}{t_{1_{cr}} + t_{2_{cr}}} \tag{3.20}$$

3.1.2 Comparison between the ideal, the measured, and the corrected frequency

Figure 3.5 shows the difference between the ideal formula of the frequency-capacitance characteristic and the new corrected characteristic taking into account the previously analyzed non-idealities.
The experimental data was taken with the BK891 impedance meter using the four-wire configuration, the sample capacitance value was obtained with a variable capacitor.
As we can see without considering the non-idealities, the frequency is overestimated and totally wrong.
The correct formula, instead, follows the experimentally measured values.
In particular we can note that in the range of interest from 100 pF to 250 pF the difference between the corrected characteristic and the experimental values is very low ($\approx$ 10 pF).

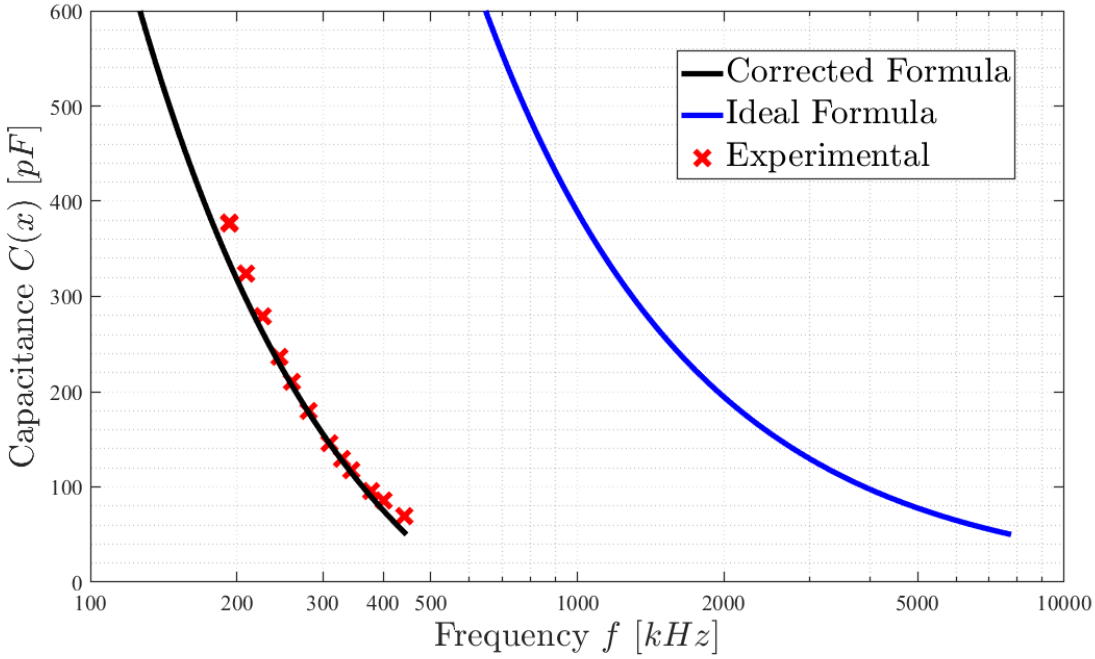

Figure 3.5. Ideal frequency-capacitance characteristic compared with the correct formula.

All the design data such as electronic circuit, component values and tolerances, data acquisition software, of the prototype necessary to obtain figure 3.5 will be explained in detail in the following paragraph.

3.2 Circuit scheme and PCB of the prototype

The basis of the circuit is the single-supply astable multivibrator as we can see in figure 3.6 where the behavior has been discussed in detail in the previous paragraphs.
In particular we have the 12 V power supply specifically chosen given that this voltage is available in the automotive sector. The 12 V power supply is also used to generate asymmetric thresholds in order to use the astable multivibrator with single supply through the resistors R_1, R_3 and R_4.
The op-amp chosen is the TLE2142, the resistors R_5 and R_6 serve as a voltage divider to reduce the dynamics of the output square wave compatible with the input dynamics of the SN74LVC1G17 schmitt-trigger which is maximum 5.5 V.
The schmitt-trigger is used as a buffer whose output is connected to the input pins of the teensy 4.0 microcontroller.
The supply voltage of the schmitt-trigger is taken directly from the microcontroller.
The following table shows all the components with their labels, values and tolerances

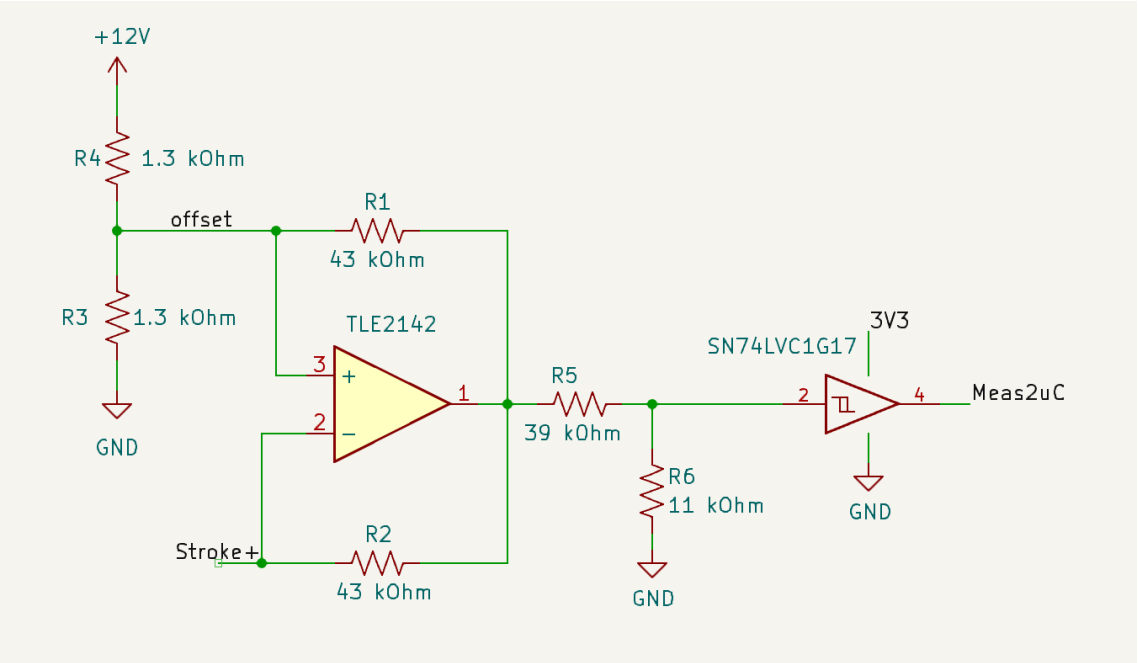

Figure 3.6. Circuit scheme of the prototype.

used for the production of PCB.

Component	**Label**	**Model**	**Value**	**Tollerance**
Op-amp	TLE2142	SOIC		
Shmitt trigger	SN74LVC1G17	SOT		
Resistor	R1	SMD	43 kΩ	±1%
Resistor	R2	SMD	43 kΩ	±1%
Resistor	R3	SMD	1.3 kΩ	±1%
Resistor	R4	SMD	1.3 kΩ	±1%
Resistor	R5	SMD	39 kΩ	±1%
Resistor	R6	SMD	11 kΩ	±1%

Table 3.1. List of components of the developed prototype.

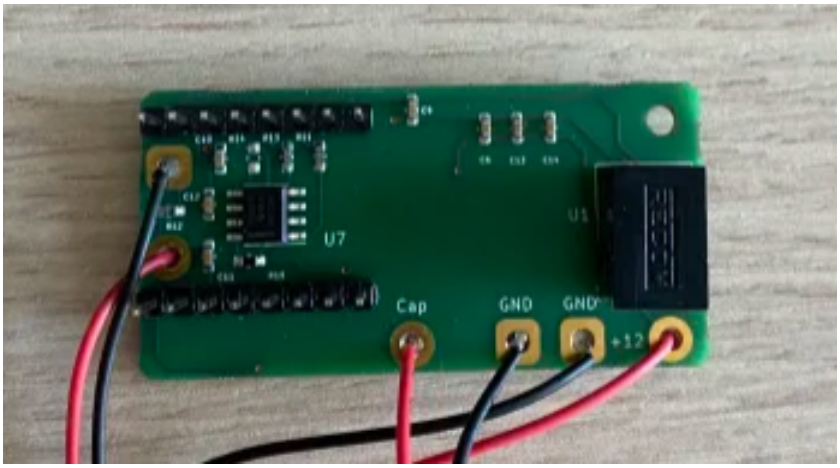

Figure 3.7. PCB of the prototype.

3.3 Microcontroller

The microcontroller used for this prototype is Teensy 4.0 with a clock frequency of 600 MHz programmed in C++.
In order to estimate the correct frequency of the signal a double interrupt is used on both rising and falling edges. Using the clock counter is simple evaluate the frequency (3.21) where f_{clk} is the microcontroller clock frequency, $cnt_{clk}(n)$ and $cnt_{clk}(n-1)$ is the value of the counter at time n and (n-1).

$$f = \frac{f_{clk}}{cnt_{clk}(n) - cnt_{clk}(n-1)} \tag{3.21}$$

Having an interrupt on both rising edge and the falling edge allows us to do a consistency check and, if the two frequency values are different, to discard the sample.
A mean over j samples can be performed to reduce the output frequency, from 100 kHz, up to CAN communication frequency, about 100 Hz, after which the position value is calculated and sent via CAN.
The μC can also perform a rolling-median and LPF. In the following paragraphs, tests with mean, median and LPF will be discussed.
After that the displacement value is calculated by passing through the frequency-capacitance characteristic and later on by the capacitance-displacement characteristic.
The final value is sent via CAN and, for testing, collect with PC using a PCAN-USB

adapter.

3.4 Software implementation for sensor testing

The sensor prototype also has ad hoc software written in C++ to perform the tests.
The software reads and writes messages in CAN-bus protocol, in this way we can have the sensor's microcontroller already programmed to communicate with the vehicle's CAN bus and simulate the acquisition by the control unit with the PC.
The value read by the software on the CAN bus is then translated into a decimal number and displayed on the screen.
The software is programmed for the real-time acquisition and display up to 4 sensors in parallel, the data acquired from each sensor are then saved in mat format convenient for reprocessing on MatLab.
The software has a "start" signal that enables the acquisition. Moreover, it presents a gain and offset values so can be varied the displacement-frequency conversion characteristic in real time directly from the test software.
Furthermore, via CAN messages it can ask the microcontroller to enable the mean of j samples on the output value, it can ask to apply the rolling-median and it can also ask to set an low pass filter LPF with a settable cut-off frequency.

3.5 Preliminary results and issues encountered during testing

Below are the main errors encountered during testing with a brief explanation of the reasons and a solution to eliminate them will be covered later.

3.5.1 Error in the frequency-capacitance characteristic

Using the correct formulas seen previously, the frequency-capacitance characteristic is very close to the measured experimental values as seen in figure 3.5.
Since the capacitance of the shock absorber is in the order of 200 pF, any source of parasitic capacitance greatly affects the total capacitance leading to an incorrect reading.
Among the capacitances that could worsen our measurements we have: parasitic capacitances due to the contact and soldering points of the components, possible interference

with the microcontroller clock signal, possible interference with the environment or with the workbench and a possible increase of capacitance caused by the cables used to connect the sensor to the shock absorber.
As we can see from the formula (2.6) an error of ±0.4 pF on the capacitance correspond to an error of ±1 mm on displacement.
Due to all the non-linearities mentioned above, our frequency-capacitance characteristic results in an error compared to the experimental value of approximately 13 pF. Which converted into an error on the position would be approximately 32.5 mm.
In the following chapters, possible solutions will be discussed and possible fine tuning will be studied to reduce the position error down to a few millimetres.

3.5.2 Temperature dependence of capacitance

Another problem encountered in the tests, which will be discussed in detail in following chapters, is the variation in capacitance as the temperature varies.
As mentioned above, the shock absorber is responsible for the conversion of kinetic energy into heat, therefore while using the vehicle the temperature of the shock absorber increases.
The starting temperature will be ambient temperature, but during winter the starting temperature could be -10 °C and the final temperature, depending on the distance travelled, can even reach 80 °C.
It is therefore necessary to precisely study the variation in capacitance as the temperature varies to allow accurate position measurement throughout the entire operating range.

3.5.3 Variable cable capacitance

To measure the capacitance of the shock absorber we need two contact points, one in the cylinder and the second one in the piston.
The relative position between cylinder and piston is not fixed in the shock absorber, therefore the connection cables with the PCB are also not fixed.
Since the cables are two metal conductors with a dielectric in between, they generate a capacitance that varies as the distance between the two wires varies.
Therefore we have an error of capacitance value that is not fixed and is not linear.
Compensating for this type of error can be very complicated and is more or less relevant depending on where the sensor is positioned and especially which contact points with the piston and the cylinder are chosen.

3.5.4 PCB component tolerances

As mentioned in the previous paragraphs, the frequency of the square wave generated by the astable multivibrator circuit is strongly affected by the non-ideal effects of the operational amplifier. The operational amplifier used in the circuit is a TLE2142 high-speed, low-noise precision operational amplifier.
The typical slew rate value is indicated in the component datasheet [TLE2142], that is different for the positive slew rate and the negative slew rate which is respectively 45 V/μs and 42 V/μs.
Since this is a typical value, it is plausible that this slew rate value may vary as the op-amp used varies. The datasheet also shows the minimum slew rate value which is 27 V/μs for both edges.
Another phenomenon reported in the datasheet is the variation in slew rate time as the temperature varies.
This uncertainty on the slew rate value between op-amps could be a problem for the repeatability of measurements with different PCBs.
The time delay can also vary between different op-amps depending on the parasitic capacitances which can vary depending on the manufacturing process.
Finally, the resistor values used to set the thresholds have a tolerance of 1%, so depending on the resistors used, different PCBs could have slightly different thresholds and generate a square wave with a different frequency.

Chapter 4

Fine tuning and linearization

To be able to make a very precise calibration of the developed prototype we need a capacitive test measurement with which to compare our frequency value later on translated into capacitance.
Among the different capacitance measurement methods we have the use of a portable LCR meter with a fixed test frequency or, as cited in [Navarun Gupta [2-4 July 2020]], the use of an un-balanced AC wheatstone bridge in which the test capacitance is measured through the use of a known capacitance by measuring an AC RMS voltage.
To have a precise measurement of capacitance depending on the test frequency we chosen to use the BK891 bench impedance meter.

4.1 Capacitance measurement with BK891

The BK891 impedance meter is a high accuracy bench LCR meter used for inductance, capacitance and resistance measurements.
The frequency span on which the impedance meter can take measurements ranges from 20 Hz up to 300 kHz.
The user manual reports an accuracy value which for our measurement ranges is 1%.

4.1.1 Calibration of BK891

The BK891 user manual requires, before taking any measurement, to carry out an initial calibration in order to have better accuracy.
In particular, it provides two different calibrations.

Figure 4.1. Impedance meter BK891.

- **Open Calibration**
  The open calibration serves to compensate for any parasitic admittance that may exist within the connection cables during testing.

- **Short Calibration**
  The short calibration compensates for any residual impedance that may exist in the cables or connections.

4.1.2 Kelvin Clip and Four-terminal sensing

In addition to the initial calibration, to improve the quality of the measurement by avoiding adding unwanted impedances, a sensing method called four-terminal sensing is used. This particular technique is used to measure electrical impedances, as mentioned in [Four-terminal], separating the cables used for current reading and voltage measurement.
In this way it is avoided that there is an added resistance given by the voltage drop on the cables which alters the value of the sample impedance.
A pair of cables called "force connections", as we can see in the figure 4.2, carry the current to the device under test, while another pair of cables called "sense connections" are placed immediately adjacent to the target impedance. Since very little current passes through

these cables, the voltage drop due to the cables is negligible.

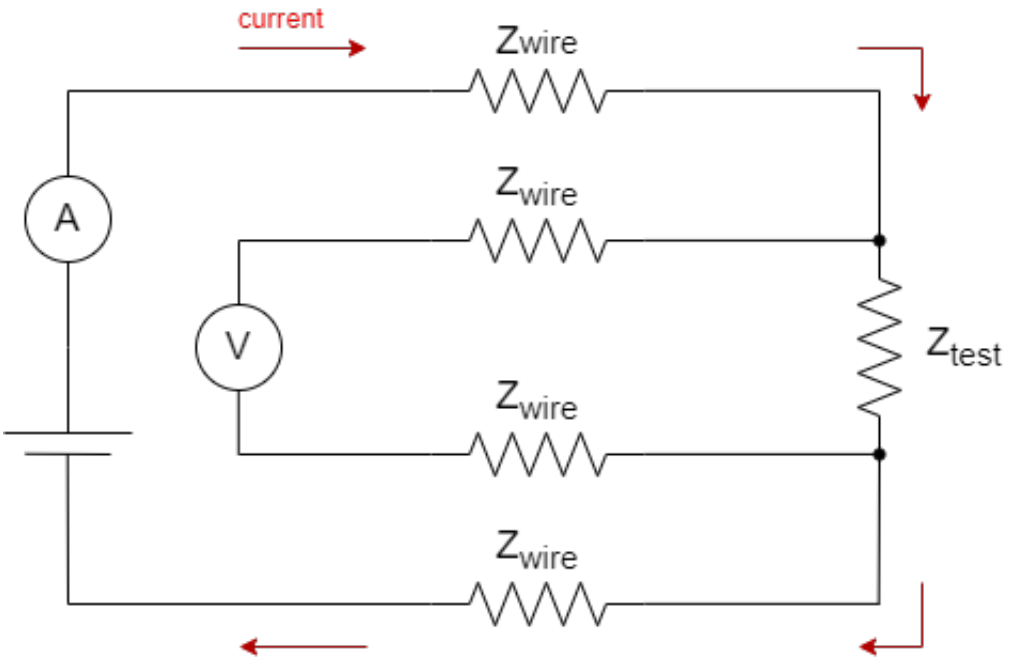

Figure 4.2. Four-wire sensing general scheme.

To make an impedance measurement using the four-terminal sensing technique we need Kelvin clips 4.4, particular clips which, as opposed to regular alligator where both jaws are connected at the connection point, in the Kelvin clip the two wires that make up the jaw are insulated. The current through the cable is called "force connections", while in the half called " sense connections" no current flows.
The general scheme of the Kelvin clips is shown in the figure 4.3.

In this way it is possible to carry out capacitance measurements by limiting the parasitic impedances of the system as much as possible.

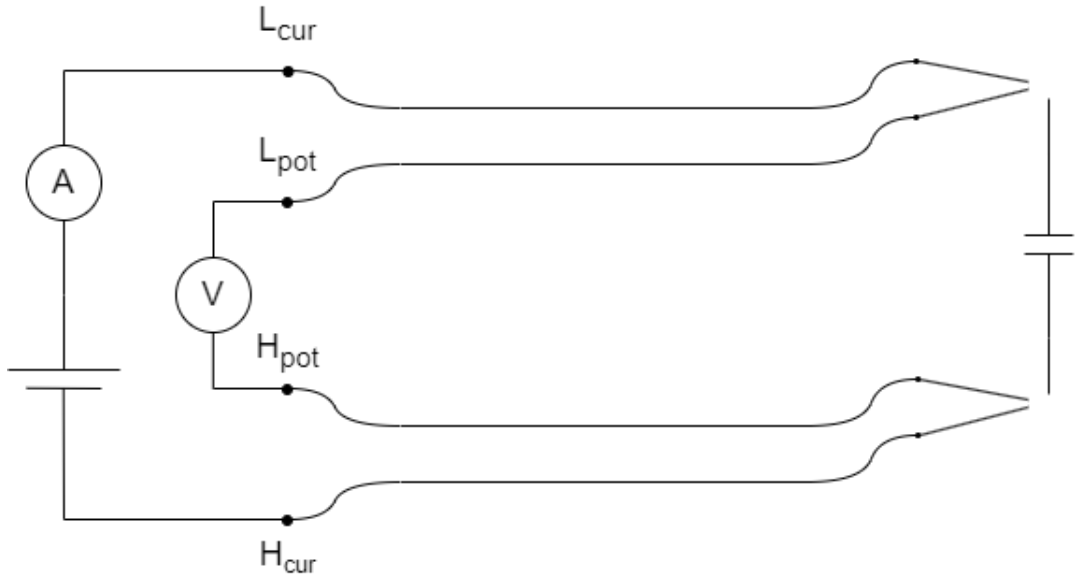

Figure 4.3. Kelvin clip general scheme.

4.2 Wire capacitance study

As mentioned previously, in the connection between the shock absorber and the PCB it is very important not to add parasitic capacitances, but since the connection cables are two close conductors with air and plastic in between acting as a dielectric, they are essentially a capacitor.
A first study was done on the connection cables used to connect the test capacitor to the PCB. The key idea is to measure the parasitic capacitance added by the cables in order to compensate it.
Using the capacitance measurement setup mentioned above, the value of several test capacitors with and without cable was measured in order to estimate their value.
The capacitance value of the test capacitors is very similar to the capacitance value of the shock absorber, in particular they are ceramic capacitors in SMD format of nominal value 220 pF at 5% tolerance NP0, so that the capacitance value was not influenced by the temperature. The table with the values of the measurements carried out are shown in the table 4.1. The uncertainty in the capacitance measurements is reported in the datasheet of the BK891, which for measurements in the order of 200 pF at a frequency of 200 kHz is 1%.

The estimated capacitance of the connection cables is 9.18 pF.
During these measurements the cables always remained in the same position and also at

Capacitor number	**Capacitor without cable [pF]**	**Capacitor with cable [pF]**	**Capacitance cable [pF]**
1	222.5	231.6	9.1
2	223.4	232.6	9.2
3	219.6	228.8	9.2
4	219.0	228.3	9.3
5	219.9	229.1	9.2
6	222.6	231.6	9.0
7	221.5	230.7	9.2
8	222.3	231.5	9.2

Table 4.1. Experimental values of 220 pF capacitors with and without cable.

Figure 4.4. Kelvin Clip.

the same distance from each other. This condition cannot be verified a priori, especially during the installation of the sensor in a real shock absorber, because the cables will be connected between the piston and the cylinder, which will move respectively during the operation of the vehicle.
It is therefore necessary to use controlled impedance shielded cables for the connection between the shock absorber and the PCB.
A low-cost option would be to use low-capacitance cables for RS-485 applications. These cables have twisted conductors to reduce electromagnetic interference (EMI), have a metal shield preventing external electromagnetic fields from affecting the measurement and whose capacitance is approximately 50 pF/m.
With the use of these cables, the problem of non-linear capacitance due to the bringing together and moving away of the conductors would be eliminated by applying only an offset, to be compensated, to the frequency-capacitance characteristic.

4.3 Fine tuning of frequency-capacitance characteristic

After estimating the capacitance value introduced by the connection cables to the PCB, we moved on to calculating the error of the measurement introduced by the frequency-capacitance characteristic with the aim of carrying out compensation and reducing the error.
The figure 4.5 shows the capacitance measurements of the same test capacitors from 220 pF at 5% tolerance and the values measured by the prototype using the frequency-capacitance characteristic defined previously.
As we can see, the measurement error is approximately 13 pF, the previously calculated offset on the capacitance introduced by the cables is 9.18 pF that partially compensates the characteristic.
There is therefore a shift in the characteristic of approximately 3.85 pF, after compensation the error between the value read by the prototype and the value measured by the BK891 impedance meter is approximately 0.2 pF.

4.4 Capacitance span measurements

After calibrating the frequency-capacitance characteristic with a fixed capacitance value, it is necessary to study the behavior and the error in a capacitance span.
The frequency-capacitance characteristic shown in the previous chapters was calculated for capacitance values ranging from 50 pF up to 600 pF. The shock absorber, during vehicle operation, oscillates around an equilibrium position, making small movements up and down. It is therefore possible to reduce the total dynamics to focus on the affected area of the characteristic.
Having assumed the central capacitance at rest of approximately 220 pF, the chosen range of interest for the measurements is between 210 pF and 230 pF. This range allows us to visualize a dynamic of approximately 5 cm around the central position.
Figure 4.6 shows the frequency-capacitance characteristic of the theoretical prototype and the experimental data in the capacitance range mentioned above.
Only the capacitance due to the contact cables with the variable test capacitor was compensated.

As can be seen, the theoretical characteristic differs from the experimental points. The error between the theoretical characteristic and the experimental values is shown in figure

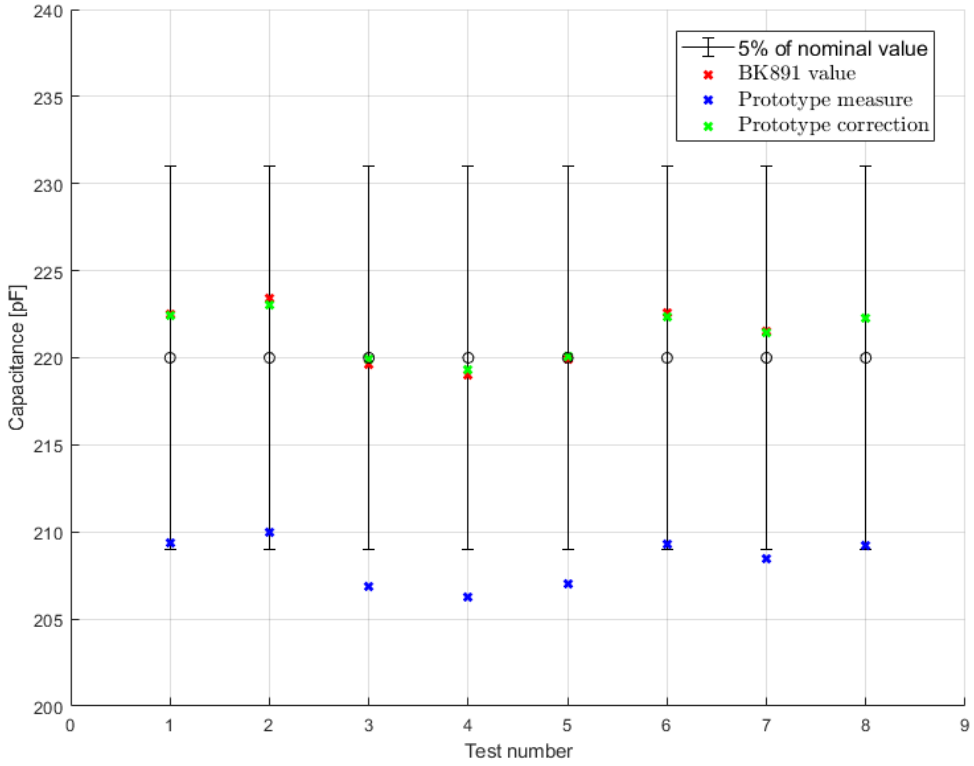

Figure 4.5. Fine tuning of frequency-capacitance characteristic with fixed capacitance.

4.7. The average error in this configuration is 3.95 pF with a maximum of 5.1 pF, which converted into position error results in an average error of 10 mm with a peak error of 13 mm.

By acting only on the offset of the characteristic, as we can see in figure 4.8, the prototype characteristic is much closer to the experimental values. Obviously, being centered at the 220 pF point, we will have a greater error as we move away from the central point. The capacitance and displacement error is shown in figure 4.9. Where it can be noted that the average error on the capacitance has decreased to 0.6 pF with a maximum of 1.3 pF. We therefore have an error on the position at the extremes of the feature of just over 3 mm.

If we act not only on the offset but also on the slope of the characteristic we obtain

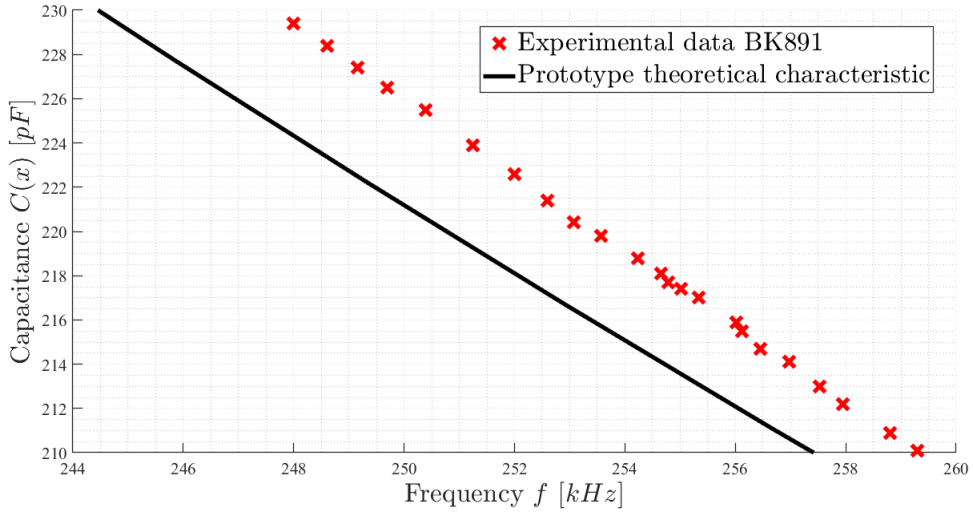

Figure 4.6. Theoretical characteristic of the prototype without correction.

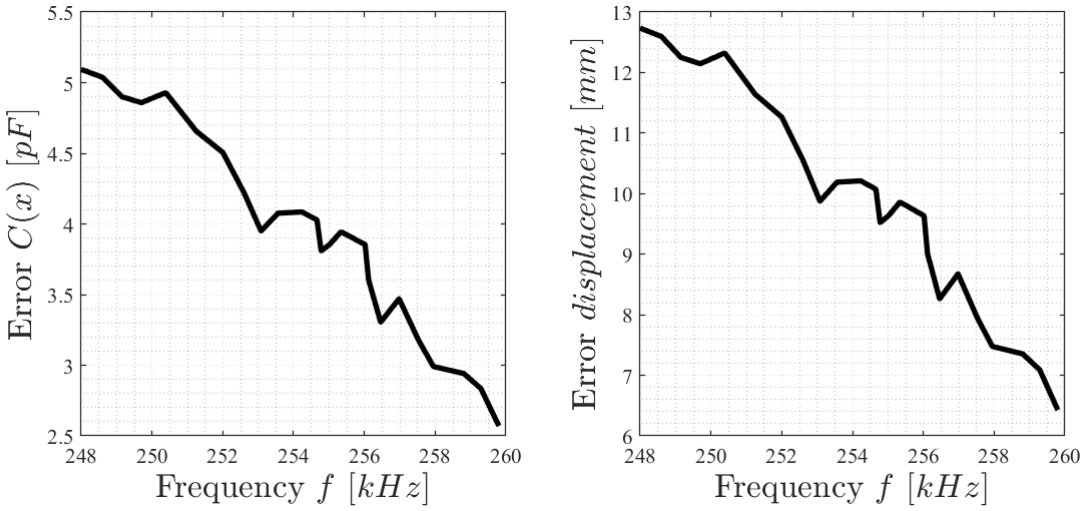

Figure 4.7. Error between theoretical characteristic and experimental value.

excellent improvements. As can be seen in figure 4.10 the frequency-capacitance characteristic of the prototype follows the experimental values very well even at the extremes of capacitance.

Figure 4.11 shows the capacitance and displacement error, the average error of which is approximately 0.1 pF with a maximum of 0.3 pF which corresponds to just under 1 mm of displacement error.

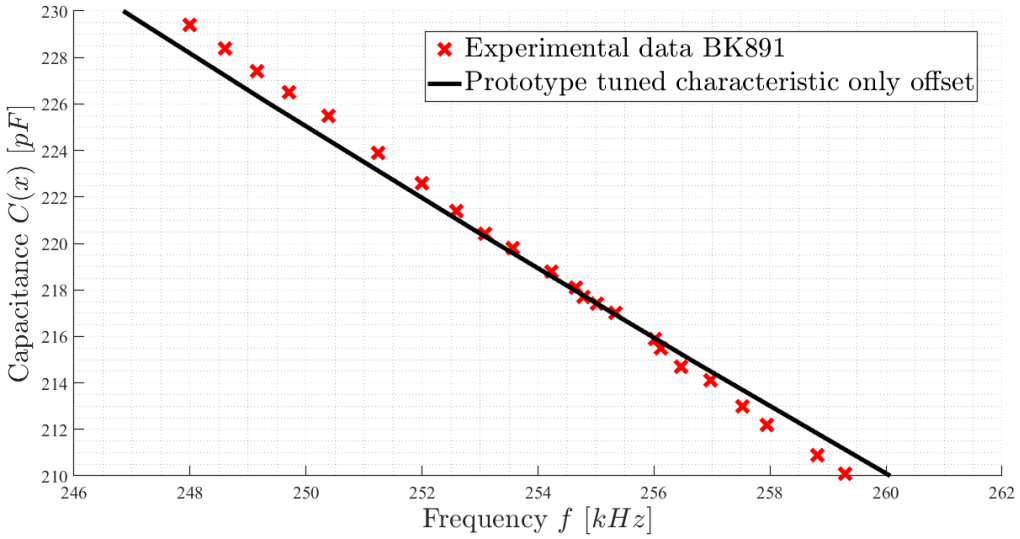

Figure 4.8. Tuned characteristic of the prototype with offset correction.

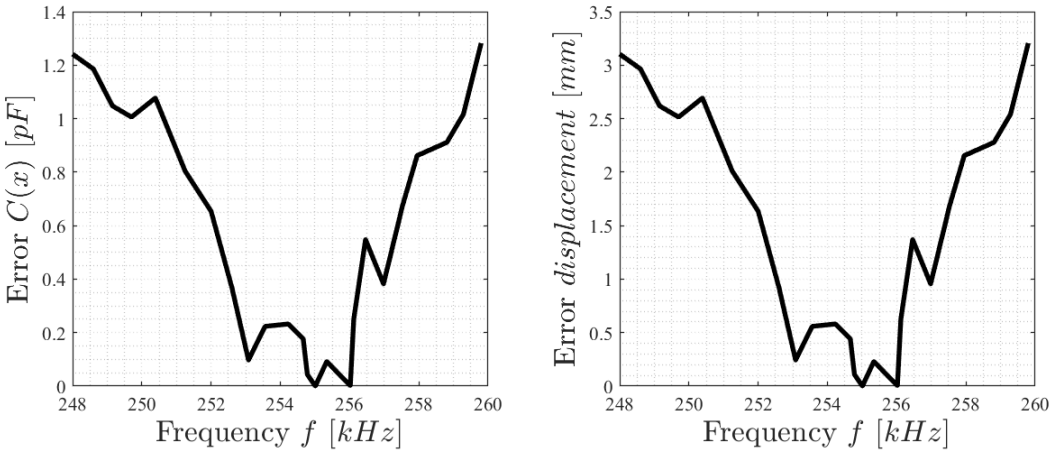

Figure 4.9. Error between the tuned characteristic with offset and experimental value.

By acting not only on the offset but also on the slope we had a notable improvement in precision. In the next paragraph several prototypes of the same PCB will be analyzed to verify if the optimizations made are valid for everyone or if an individual calibration is necessary due to the tolerances of the components.

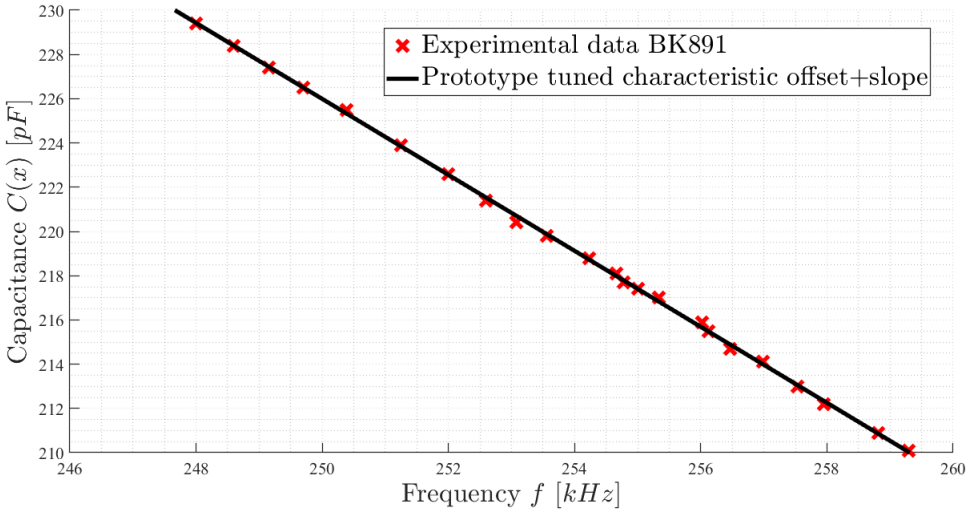

Figure 4.10. Tuned characteristic of prototype with offset and slope correction.

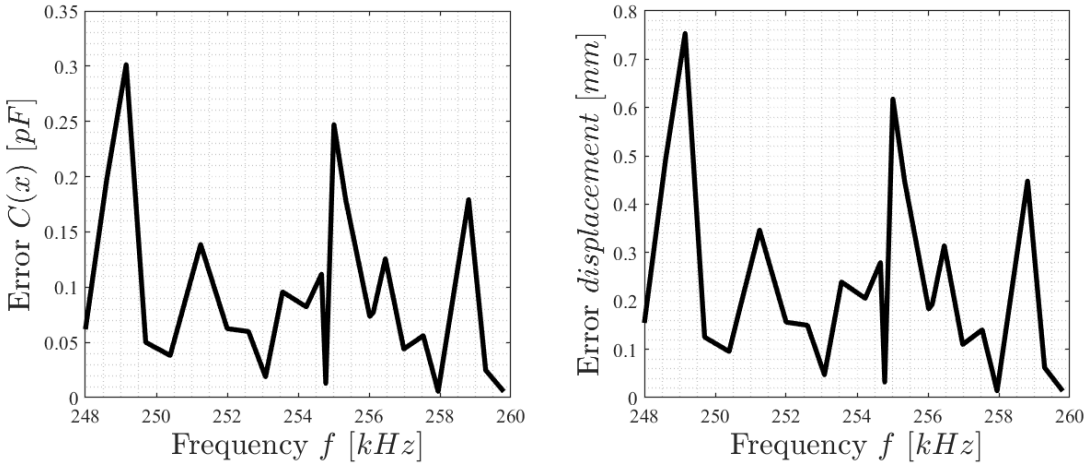

Figure 4.11. Error between the tuned characteristic with offset and slope and experimental value.

4.5 Repeatability test with different prototypes

To study the repeatability of the measurements, a second PCB was made with the same components and the same measurements were performed.
To connect the PCB with the variable capacitor the same cable used for the first prototype was used. In this way the characteristic is already compensated with the capacitance value introduced by the cables.

The span of measured capacitance is from 210 pF up to 240 pF. All measurements were performed under the same conditions as the previous test in order to be able to compare the results.
As we can see in figure 4.12, the frequency-capacitance characteristic of the second prototype is different from the experimental values.
In figure 4.13 we can see the error between the theoretical characteristic and the experimental values which turn out to be up to 8 pF at the extremes of the characteristic.
Translating into a maximum error of 20 mm on the displacement with an average error of 13.7 mm.

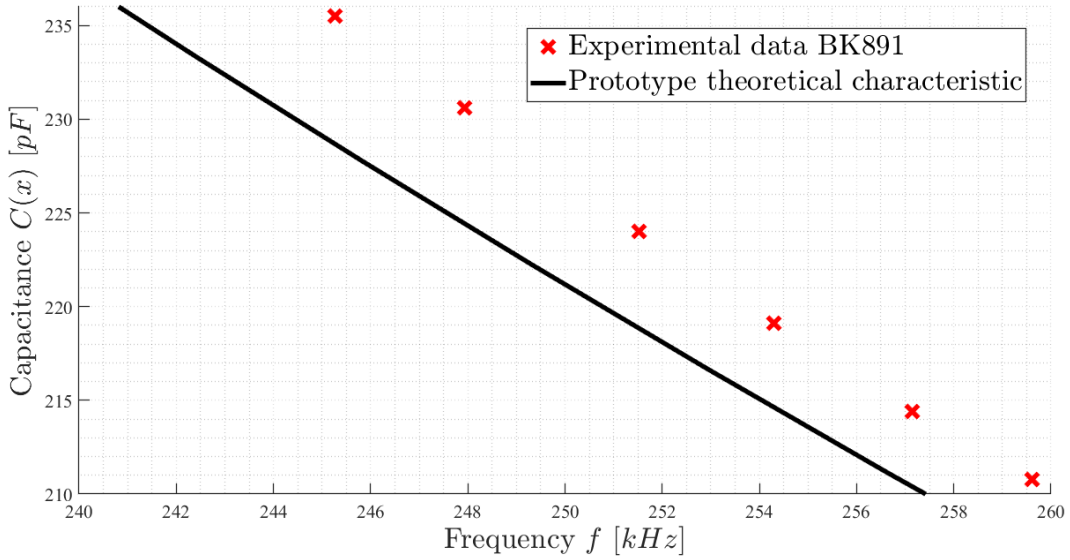

Figure 4.12. Theoretical characteristic of prototype without correction in PCB #2.

By applying the same offset calculated previously to the characteristic we obtain clear improvements as we can see in figure 4.14.
In particular, in figure 4.15, a maximum error on the capacitance of 4 pF which corresponds to a maximum error on the displacement of 10 mm, the average error in this case is 4 mm.

Finally, acting on both the offset and the previously calculated slope, the frequency-position characteristic follows the experimental values quite precisely figure 4.16.
The maximum capacitance error, shown in figure 4.17, is 2.2 pF.
The average error on the displacement compared to the experimental values is therefore

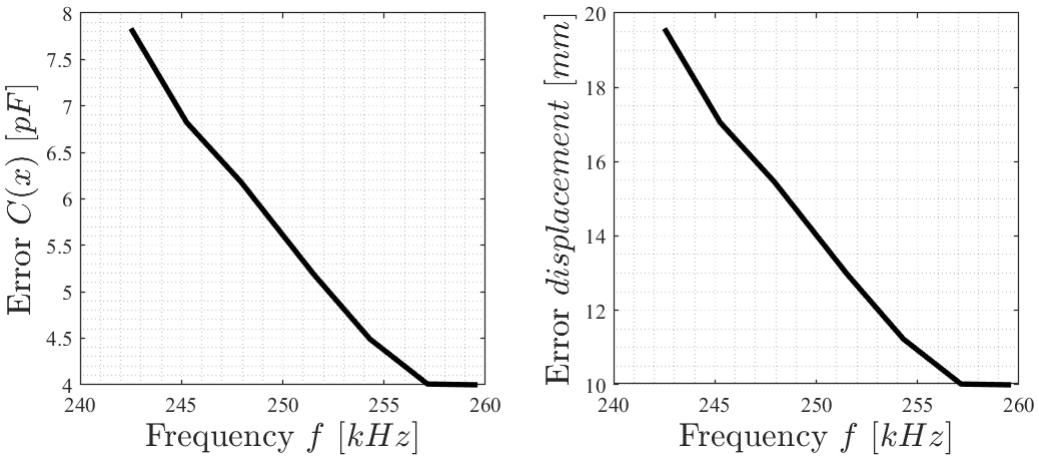

Figure 4.13. Error between theoretical characteristic and experimental value in PCB #2.

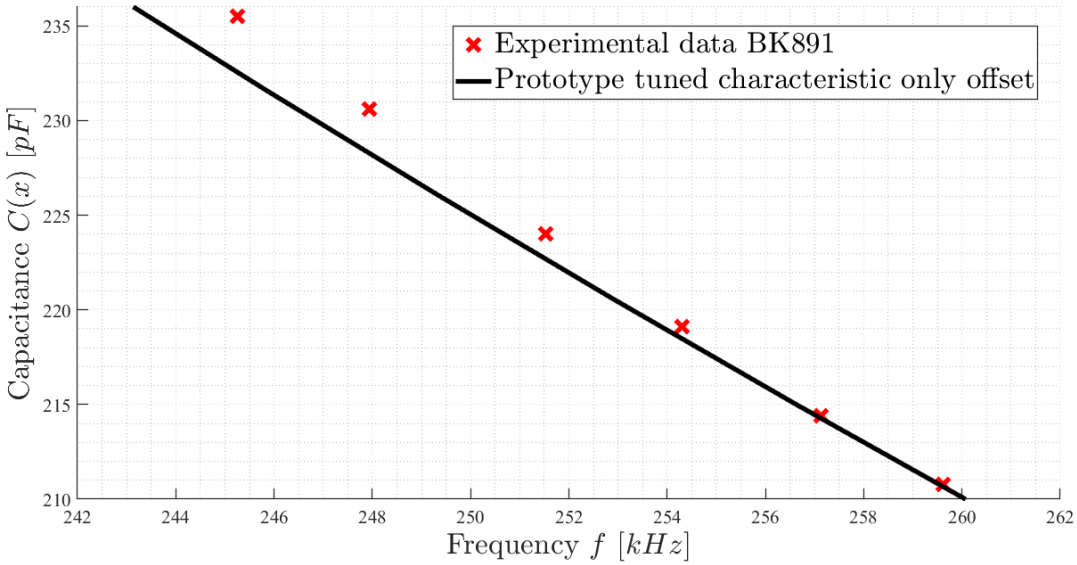

Figure 4.14. Tuned characteristic of prototype with offset correction in PCB #2.

2.7 mm with the maximum of 5.5 mm at the extremes of the characteristic.

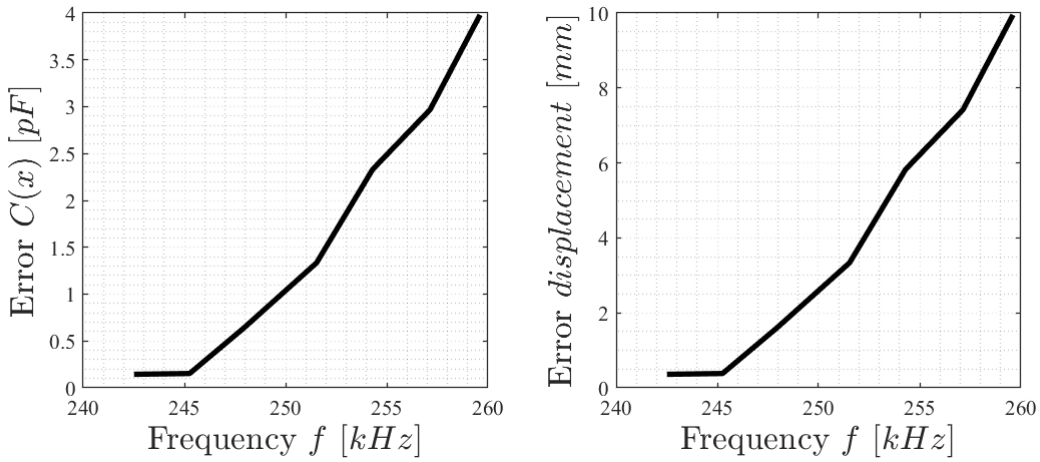

Figure 4.15. Error between the tuned characteristic with offset and experimental value in PCB #2.

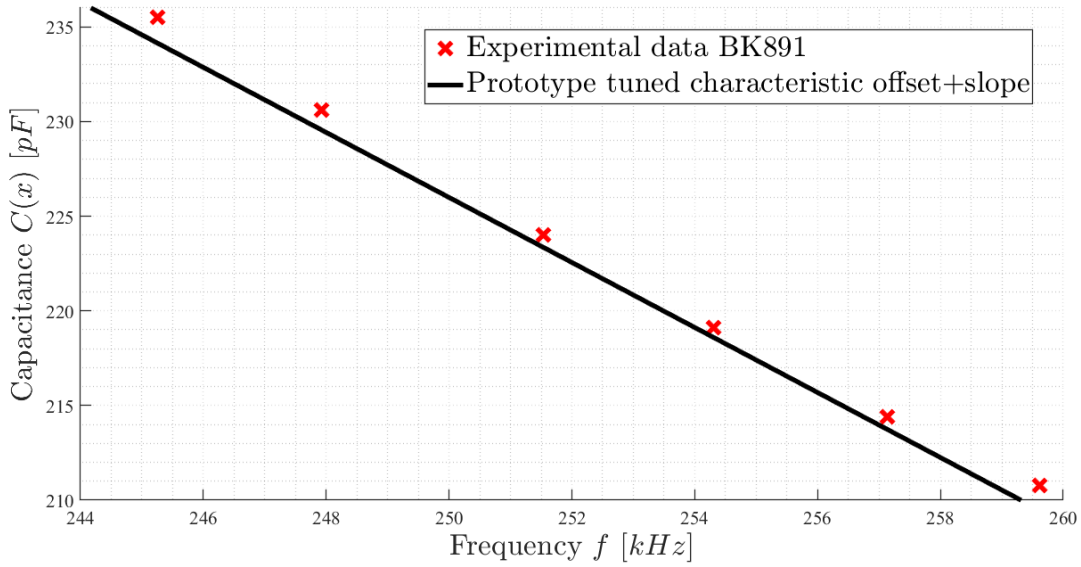

Figure 4.16. Tuned characteristic of prototype with offset and slope correction in PCB #2.

4.6 Repeatability in time

The following test was done 2 days after the first in order to study the repeatability of the measurements.

The second test was done in the same conditions as the previous one, using the same connection cables on the same workbench.

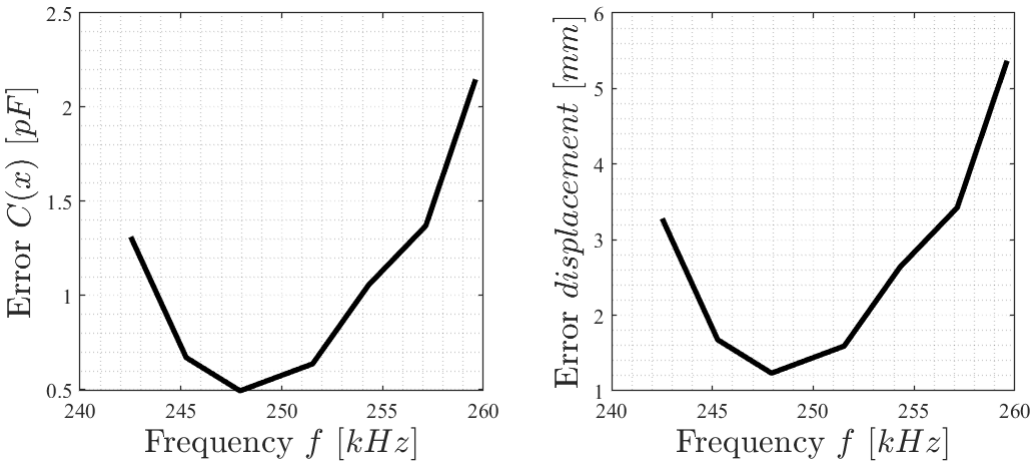

Figure 4.17. Error between the tuned characteristic with offset and slope and experimental value in PCB #2.

As we can see from the 4.18 figure, the frequency read by the prototype is slightly different compared to the first test.
In particular, as can be seen in figure 4.19, without any correction to the characteristic we have an error of 18 mm, while the previous test in these conditions highlighted a maximum error of 13 mm.
Between the first test and the second test, a difference in the frequency and therefore capacitance reading of approximately 2 pF was found.

Applying the same offset corrections, figure 4.20, we have a maximum error of 10 mm and an average error of 3.8 mm.
By acting on both the offset and the slope, as seen in figure 4.22, the maximum error is reduced to 4.5 mm with an average error of 2.5 mm.

The error measured by the same sensor after a few days worsened by 1.5 mm. This may be due to the temperature difference at which the tests were performed. By varying the dielectric constant, in this case of the air, as the temperature varies and consequently the capacitance.
Table 4.2 shows the maximum and average error values for the theoretical characteristic, for the characteristic compensated only with the offset and for the characteristic compensated with offset and slope.
Another phenomenon that could have worsened the measurement is a drift phenomenon which will be analyzed in the following paragraph.

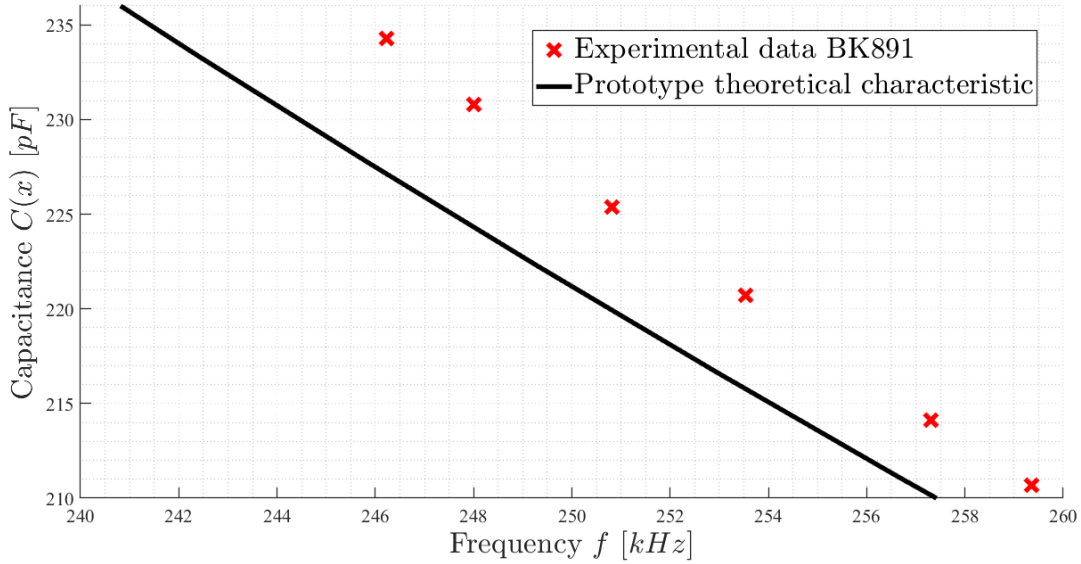

Figure 4.18. Theoretical characteristic of prototype without correction.

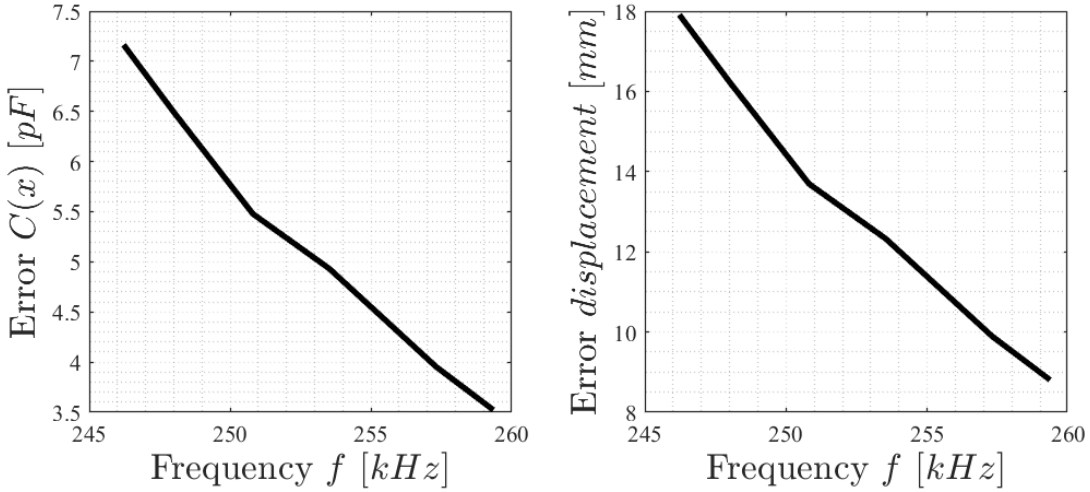

Figure 4.19. Error between theoretical characteristic and experimental value.

	Prototype #1	**Prototype #1 Test 2**	**Prototype #2**
Maximum error in theoretical characteristic	12.7 mm	17.9 mm	19.5 mm
Mean error in theoretical characteristic	9.8 mm	13.1 mm	13.7 mm
Maximum error with offset compensation	3.2 mm	8.3 mm	9.9 mm
Mean error with offset compensation	1.5 mm	3.8 mm	4.1 mm
Maximum error with offset and slope compensation	0.7 mm	4.5 mm	5.3 mm
Mean error with offset and slope compensation	0.3 mm	2.6 mm	2.7 mm

Table 4.2. Errors in tests with different compensation methods.

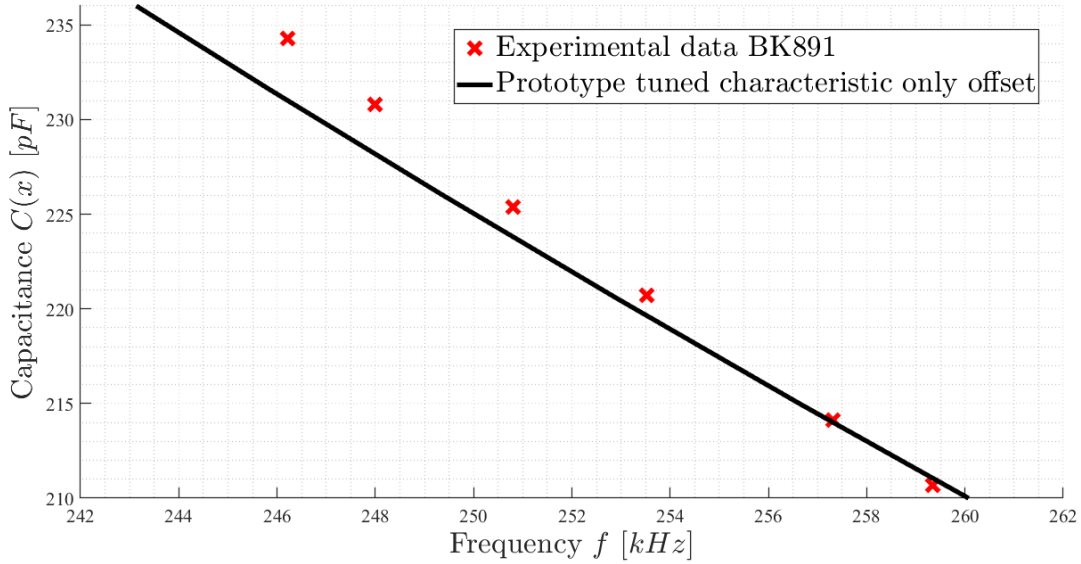

Figure 4.20. Tuned characteristic of prototype with offset correction.

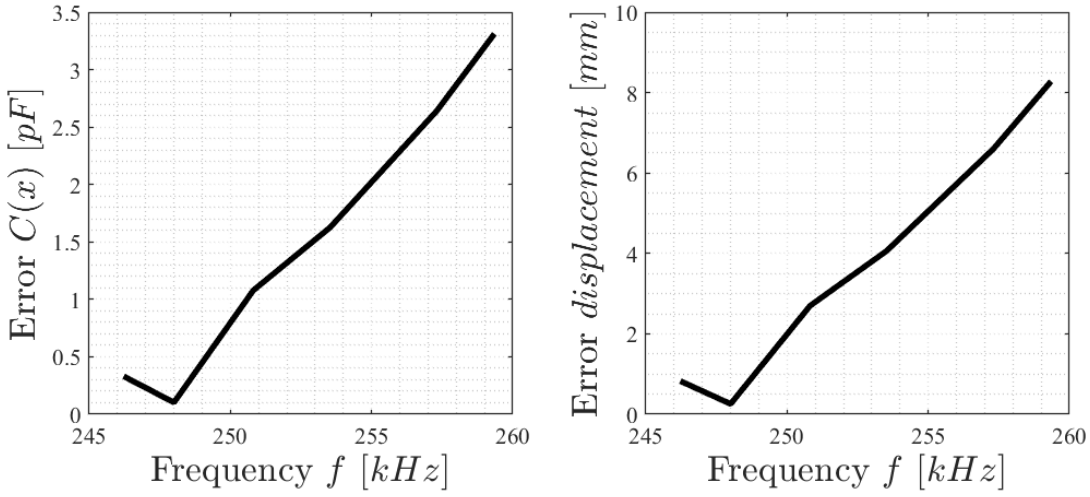

Figure 4.21. Error between the tuned characteristic with offset and experimental value.

4.7 Initial drift in frequency measured

An initial drift behavior was also observed on both prototypes as we see in figures 4.24 and 4.25. This behavior, which disappears after about 20 minutes, could be caused by temperature variations during use of the circuit.

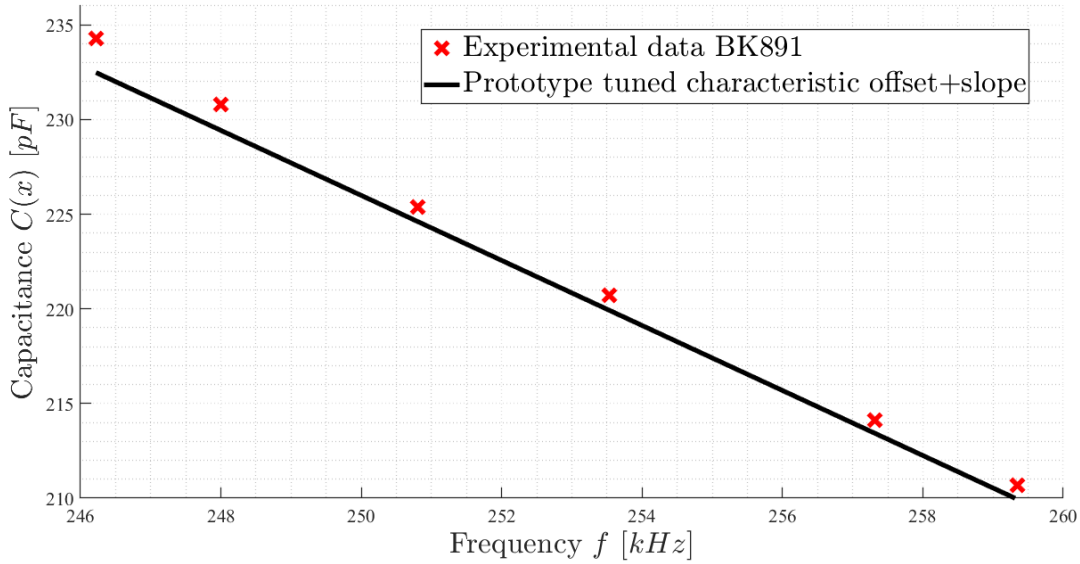

Figure 4.22. Tuned characteristic of prototype with offset and slope correction.

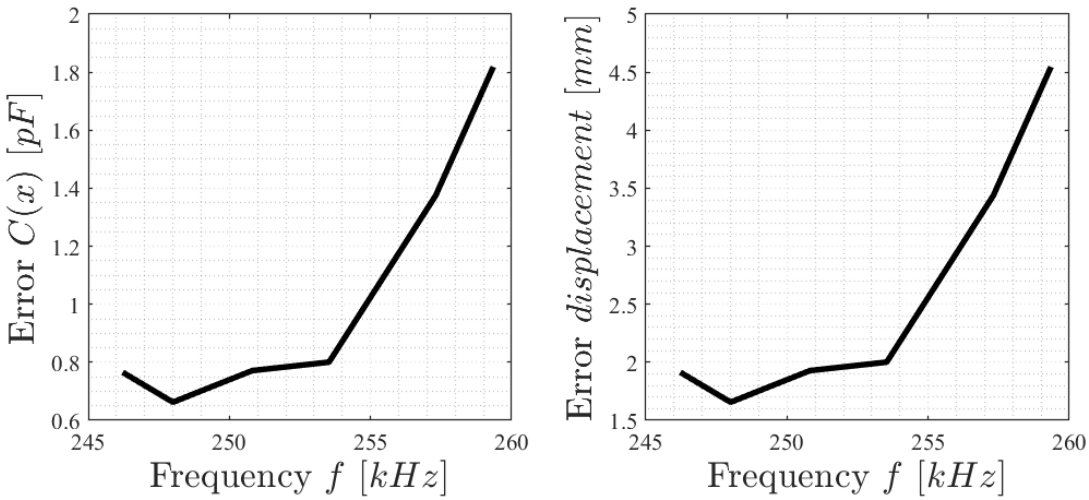

Figure 4.23. Error between the tuned characteristic with offset and slope and experimental value.

This initial drift could be caused by thermal phenomena of the PCB which influence the time delay and slew rate values of the op-amp.
To reduce this contribution as much as possible, a first solution is to leave the sensor switched on during all the measurements, in this way, since the sensor does not have to

be turned off and on again, the drift transient can be considered extinguished after approximately 20 minutes.

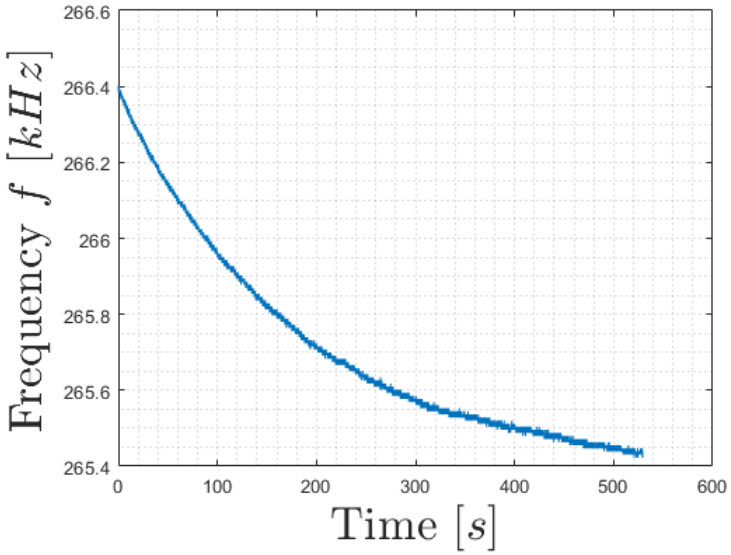

Figure 4.24. Drift in time of BCB #1.

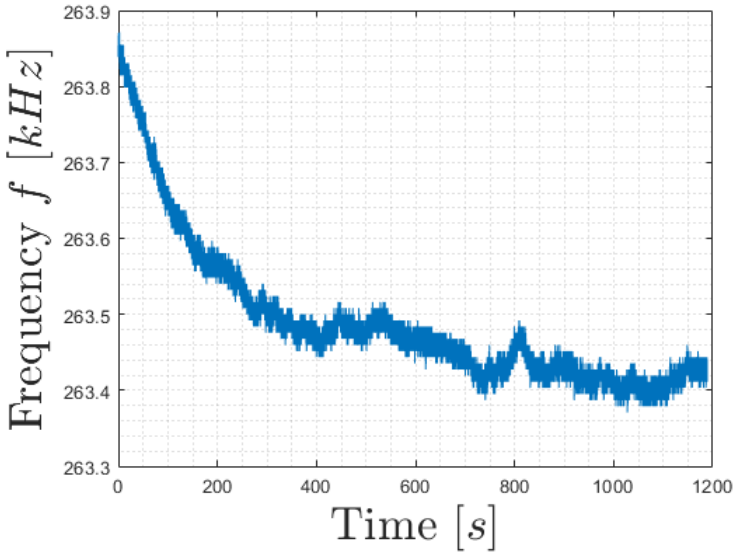

Figure 4.25. Drift in time of BCB #2.

4.8 Final calibration conclusions

We can see how, as the PCB varies, there is a different frequency reading, and consequently capacitance. Probably due to component tolerance and thermal phenomena.
Furthermore, a difference in readings of the same prototype was observed after several days, probably due to the difference in temperature of the two tests.
A possible solution for the difference in readings between the various PCBs can be an initial calibration of the sensor.
By adding a calibration state to the microcontroller, the capacitance of the shock absorber in full extension and full compression could be measured in order to calibrate the characteristic according to the sensor.
In this way the problem of tolerances of the PCB components would be eliminated and the displacement error read between one sensor and another would be reduced.
The influence of temperature on measured capacitance will be discussed in detail in the next chapter.

Chapter 5

Temperature dependence of the dielectric constant of the oil

As mentioned above, the purpose of the shock absorber is to convert kinetic energy into heat. But as we saw in the previous chapter, the capacitance value is strongly influenced by temperature.
It is therefore essential to study the variation in capacitance as the temperature varies. In particular, the quantity that varies with temperature is the dielectric constant of the material that acts as a dielectric, in our case synthetic oil.
The article [A. A. Carey] shows the variation of dielectric constant as a function of temperature of different paraffinic hydrocarbons. In particular, according to this article, the paraffinic hydrocarbons examined have a decrease in dielectric constant between 0.0013 and 0.05 per degree °C.
In the following paragraph, the variation of the dielectric constant of the oil used in the shock absorber will be studied in a temperature range between -10 °C, simulating a departure in winter, and 80 °C being the temperature that shock absorber reaches after some hours of travel.

5.1 Creating a test capacitor

To study the variation of the dielectric constant of the oil with temperature was created a capacitor with parallel plate custom-cut from an iron sheet kept separate by a 3D-printed support.

The dimensions of the bars are 153 mm x 57 mm spaced 1 mm from each other.
The capacitor was later immersed in a tray containing the oil under test whose dielectric constant value was approximately 2.2.

Once the physical dimensions of the capacitor and the dielectric constant of the oil are

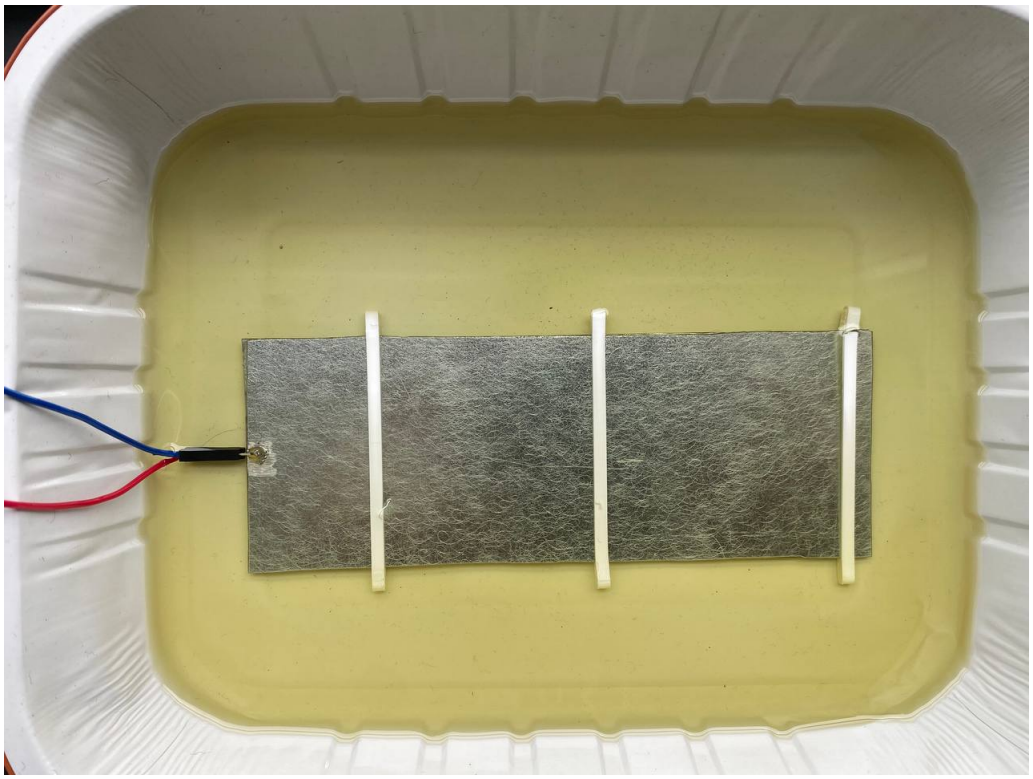

Figure 5.1. Custom-made parallel plate capacitor.

known, the capacitance can be estimated using the previously mentioned formula for a parallel plate capacitor (2.1).
The estimated capacitance, according to the formula, is approximately 175 pF at 20°C.
To experimentally measure the capacitance of the created capacitor was used the prototype of the sensor under development previously calibrated according to the results obtained in the previous chapter.
The capacitance value measured by the sensor is approximately 175 pF which coincides with the previously calculated theoretical value.

5.2 Temperature measurement

The temperature was taken using a K-type chromel-alumel thermocouple with a Seebeck coefficient of $41\mu V/°C$.
The thermocouple voltage was measured with the 34401A digital multimeter connected via RS232 serial protocol to MatLab in order to acquire voltage measurements with a frequency of approximately 1 Hz.
The voltage measurement was later on converted into temperature.

5.3 Data acquisition and results

To acquire the capacitance values, the prototype was set so that it made 100 measurements per second averaging the other samples.
The complete setup for data acquisition is shown in figure 5.2.

The tray containing the capacitor and the test oil was cooled and heated on a heating plate from -10°C up to 80°C.
The following figures show the capacitance results as a function of temperature variation 5.3 (A).

Later on, the dielectric constant was calculated from the capacitance value and the following figure shows the variation in the dielectric constant of the oil as the temperature varies 5.3 (B).

The capacitances involved, which are in the order of 175 pF, and the uncertainties of the measuring instruments mean that between one measurement and another there is a minimal variation in capacitance and consequently in the measured dielectric constant.
We therefore repeated the measurement several times to try to understand and estimate the uncertainty value of the capacitance value and dielectric constant.
In particular in the figure 5.4 the variation in capacitance with respect to temperature in six different tests, all performed with the same methodology but on different days.
As can be seen, the uncertainty on the capacitance is approximately $\pm 1pF$. The figure 5.5 shows the variation in the dielectric constant of the oil as the temperature varies in the respective tests.

As we can see from these first tests, the variation in dielectric constant as a function

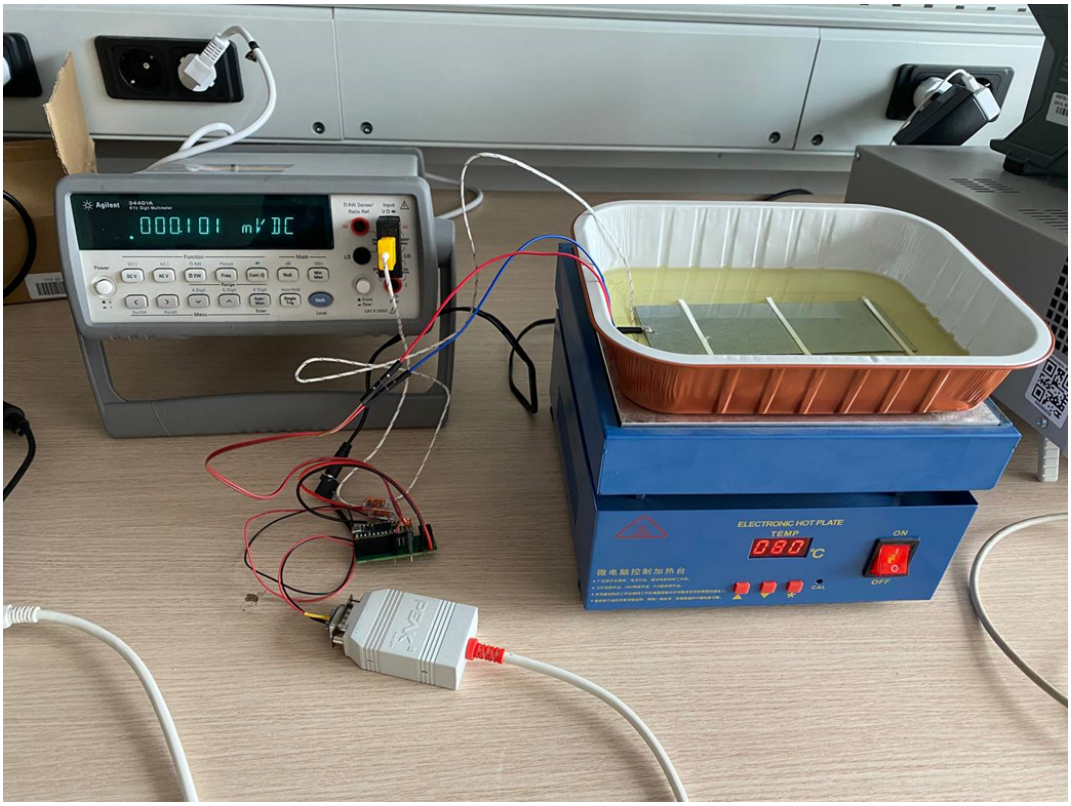

Figure 5.2. Setup for the measurement of dielectric constant as a function of temperature.

of temperature is not very linear. A possible problem could be due to the uneven distribution of heat passing from the plate to the oil.
The oil temperature is taken with a thermocouple fixed in the middle of the oil. But the heat coming from below generates a temperature gradient.
A solution to this problem could be to increase the quantity of oil in the tray so that the temperature increases more evenly. In the next paragraph the results obtained from the new tests will be analyzed and discussed.

5.4 Testing increasing oil quantity

The following tests were carried out with the same setup. The connection cables between the capacitor and the prototypes are always the same, the cooling down to -10 °C and the heating up to 80 °C occurred with the same methodology reported in the previous paragraph.

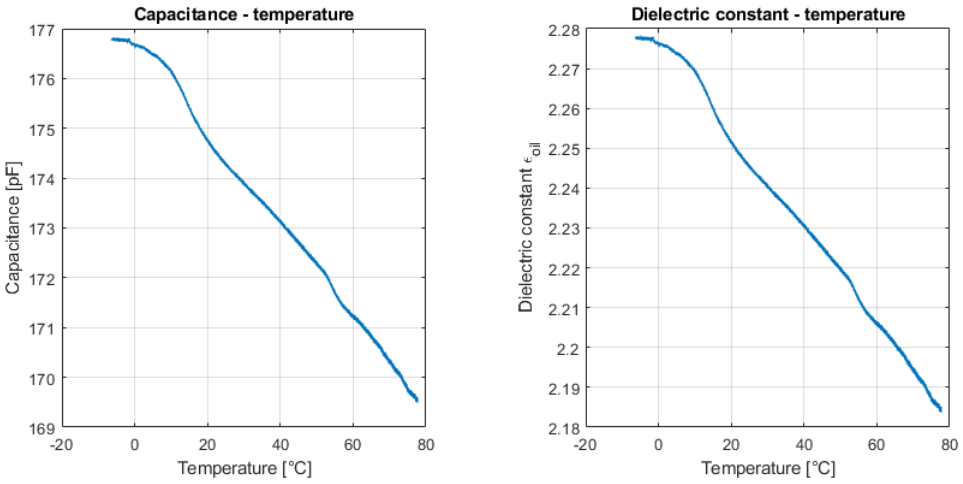

Figure 5.3. A) Capacitance vs temperature characteristic. B) Dielectric constant vs temperature characteristic.

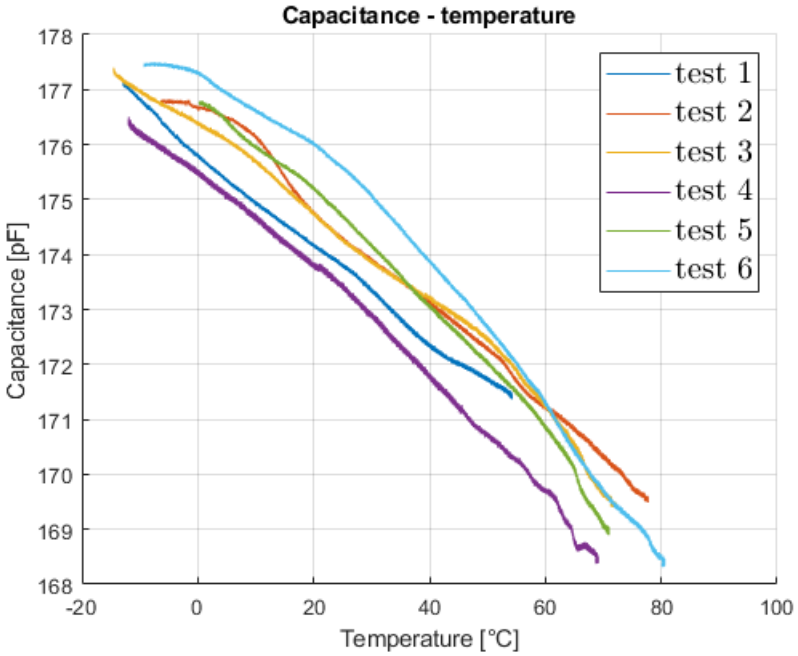

Figure 5.4. Capacitance vs temperature characteristic over six tests.

The only difference is in the quantity of oil used as a dielectric in order to make the temperature variation inside the oil as homogeneous as possible.

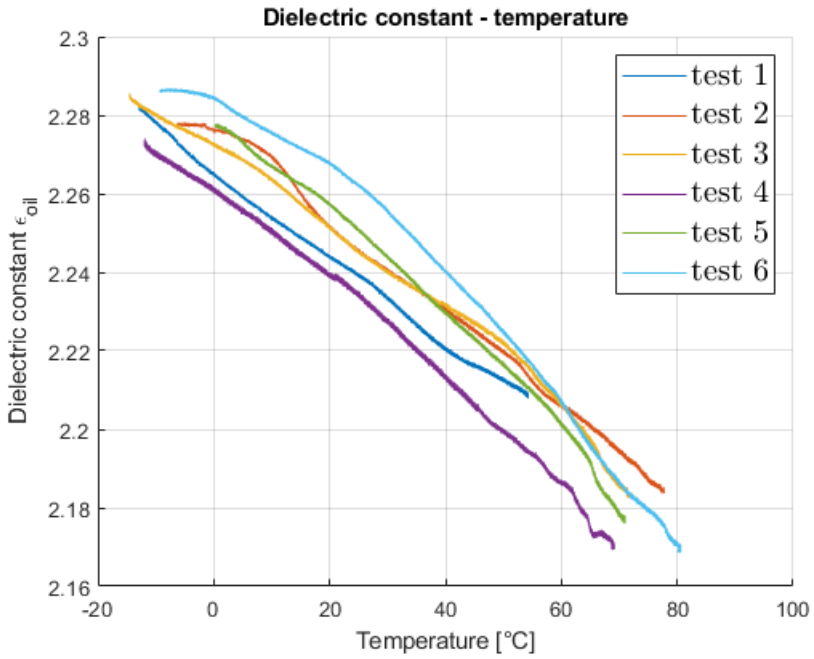

Figure 5.5. Dielectric constant vs temperature characteristic over six tests.

As we can see in the figure 5.6 the dielectric constant-temperature characteristic is more linear as had been hypothesized.

Increasing the quantity of oil present in the tray decreased the uncertainty on the capacitance measurement, making the different tests more coherent.
We can then take an average between the various tests and linearize the characteristic.

5.5 Linearization of the dielectric constant characteristic as a function of temperature

The linearized characteristic in the figure 5.7 was obtained by averaging the values calculated with the different prototypes and later on linearizing the obtained function to the first order.
The slope of the line is 0.0012. Therefore the dielectric constant of the oil drops by approximately 0.0012/°C.
The value found is perfectly aligned with the typical values of dielectric constant variation

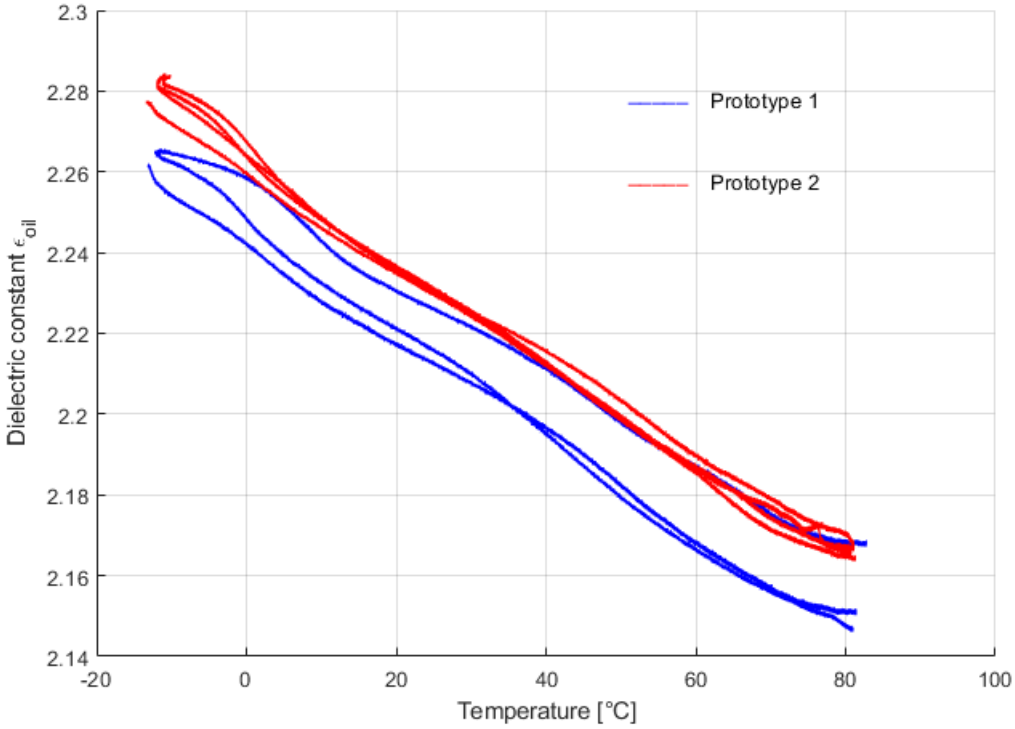

Figure 5.6. Capacitance vs temperature characteristic after increasing the oil quantity.

of synthetic oils.

The dielectric constant value at temperature of -10 °C is approximately 2.27. While at 80 °C we have a value of 2.16.
The dielectric constant variation in a temperature range of 90 °C is 0.11.
In the next paragraph the impact of this difference in dielectric constant on the capacitance measurement and on the displacement calculation in the shock absorber will be analyzed.

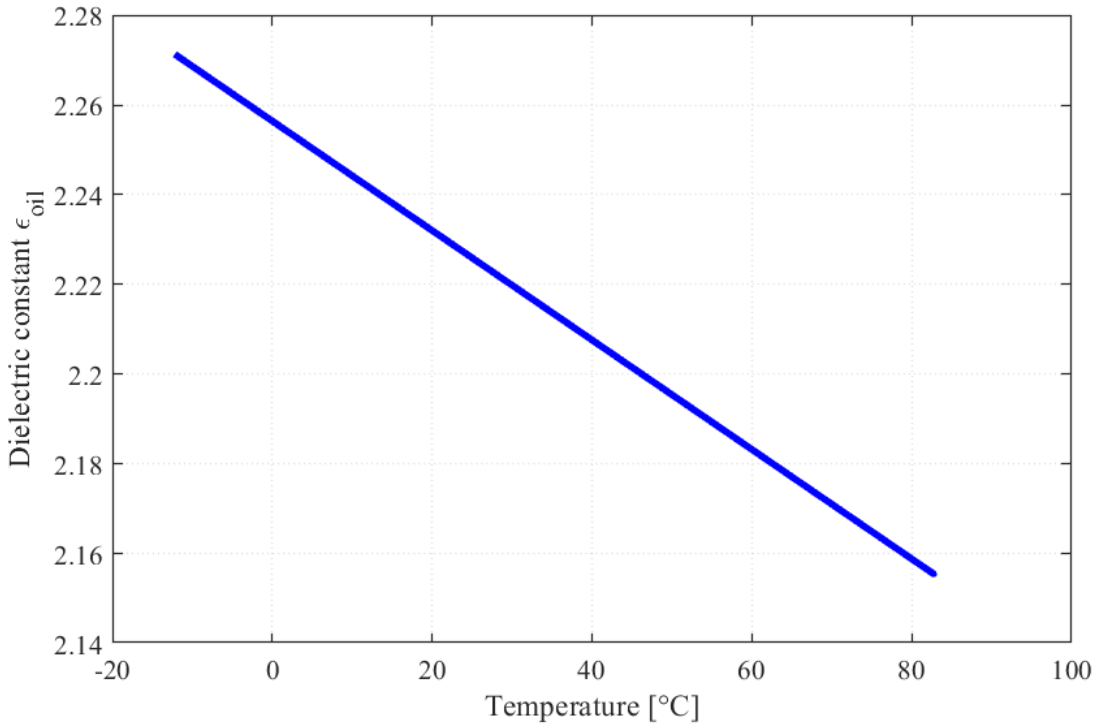

Figure 5.7. Linearization of dielectric constant-temperature characteristic.

5.6 Impact of temperature on position measurement in the shock absorber

In this paragraph the impact of the variation of the dielectric constant of the oil in the shock absorber as the temperature varies with respect to the measured displacement will be evaluated.

The variation of dielectric constant changes the capacitance value of the shock absorber and consequently the measured displacement. Knowing how the capacitance varies as a function of temperature allows us to compensate the characteristic in order to measure the displacement more precisely.

After measuring the variation in the dielectric constant of the oil we can insert it into the formulas for calculating the capacitance-displacement characteristic.

The capacitance-displacement characteristic, by inserting the temperature dependence of the dielectric constant, passes from (2.4) to (5.1) where $\epsilon_{oil}(T)$ is the characteristic shown in the figure 5.7.

$$C(x) = C_0 + \frac{2\pi\epsilon_{oil}(T)\epsilon_0 x}{ln(\frac{r_2}{r_1})} + \frac{\pi\epsilon_{oil}(T)\epsilon_0(r_3)^2}{l - x - l_1} + \frac{\pi\epsilon_{oil}(T)\epsilon_0(r_3 - r_4)^2}{x} \tag{5.1}$$

We can therefore calculate the new function that links capacitance and displacement in order to calculate the change in capacitance of the shock absorber as the temperature varies and return a correct displacement value.
The figure 5.9 shows the difference in the curve at the extremes of the temperature dynamics. Assuming that the shock absorber has a capacitance of 220 pF in the rest position. We can see that between the curve at -10 °C and the curve at 80 °C we have a difference in capacitance for the same displacement of approximately 1.5 pF.

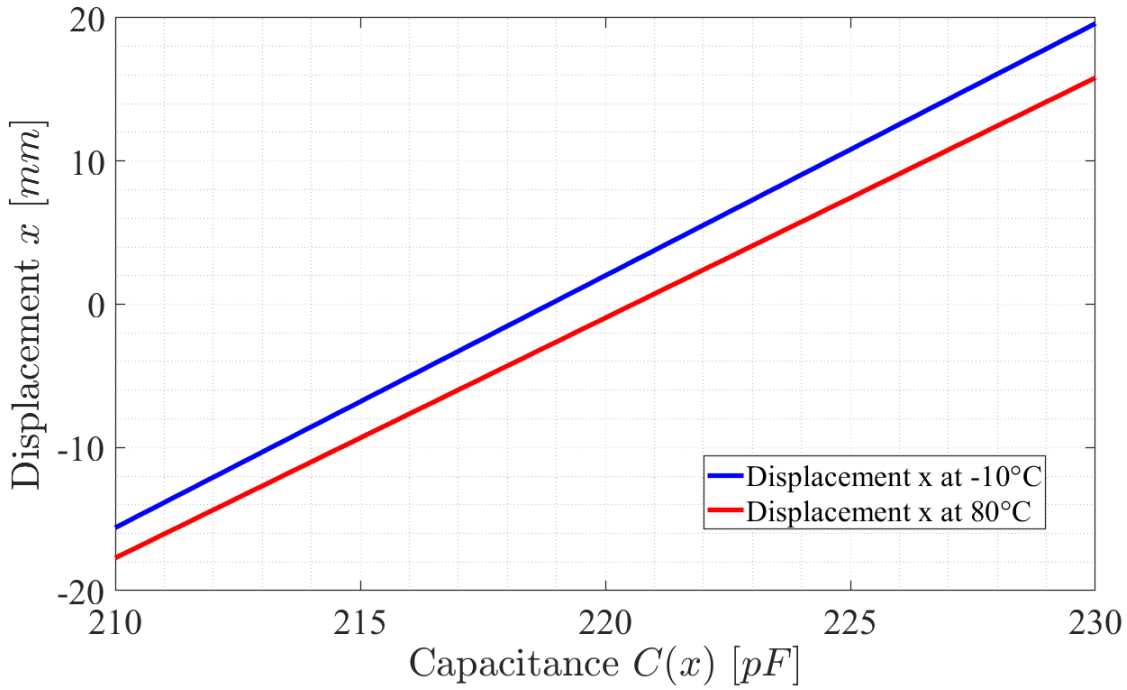

Figure 5.8. Displacement-capacitance characteristics at different temperature.

The figure 5.9 shows the final characteristic between displacement and frequency measured by the position sensor at different temperatures.
To obtain this characteristic, the linearized characteristic between capacitance and frequency discussed in chapter 4 and the linearized displacement-capacitance characteristic discussed in chapter 2 were used.

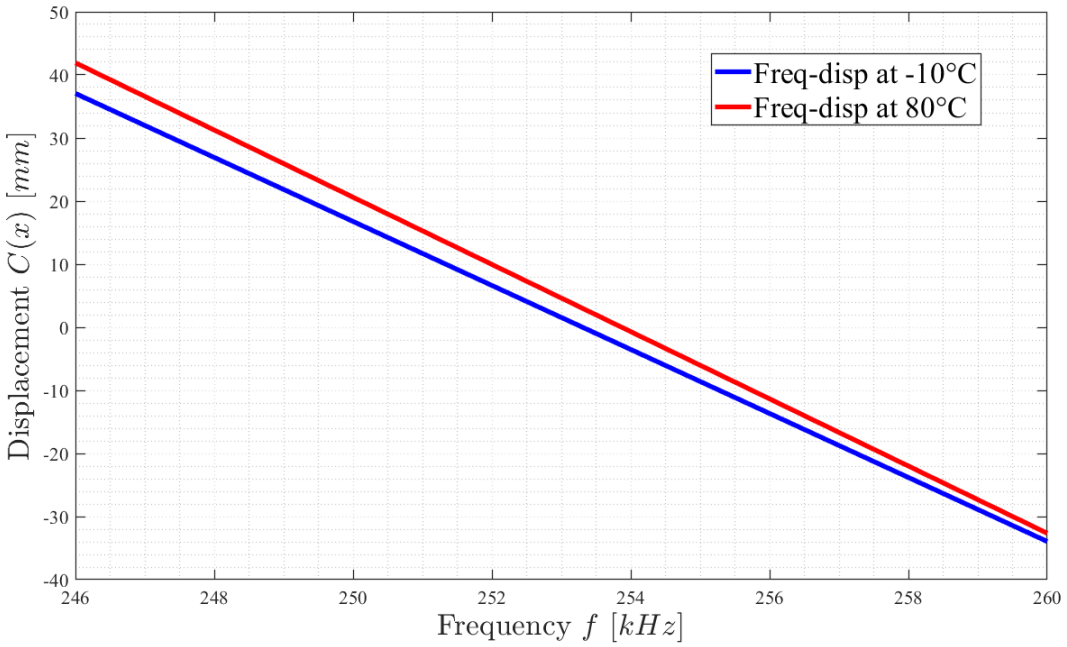

Figure 5.9. Frequency-displacement characteristics at different temperature.

As we can see, the temperature plays a fundamental role in the capacitance value of the shock absorber. If the temperature contribution is not considered, on average an error of 4 mm is made on the position value.
To be able to implement temperature dependence in the sensor it would be sufficient to add a temperature sensor connected to the microcontroller in order to read the temperature of the shock absorber in real time, which being made of ferromagnetic material will have good thermal conductivity, in order to compensate for the characteristic.

Chapter 6

Static and dynamic tests

In this chapter we will see the static and dynamic tests and we will see the difference of the various filters that can be set in the sensor including the mean, the rolling-median and the low pass filter with settable frequency.
For these tests, prototype number 1 was used and the variable capacitor was used in order to simulate the capacitance of the shock absorber.
The purpose of this chapter is to understand the best sampling configuration and the right filter combination that is most functional. Finally, being able to determine if the sensor can follow the dynamics of a shock absorber in normal road use.

6.1 Static tests

For the static test the variable capacitor was set to a fixed capacitance in order to simulate the shock absorber with a fixed displacement value of approximately 54 mm.
We then acquired the data in different configurations for 10 seconds and plotted the graphs. In this test the prototype was tested without any type of filter, the use of the mean, the use of the median of 3 samples, the use of mean and median and finally the use of mean, median and low pass filter with cut-off frequency of 100 Hz.
The sampling frequency of the microcontroller is 100 kHz.
In figure 6.1 we have sampling without any type of filter applied. As we can see the sampled value oscillates around the position of 54 mm and is very dirty and noisy.
By meaning the samples, as seen in the figure 6.2, the sampling is much cleaner and less noisy, significantly increasing the quality of the measurement.
Using only the median on 3 samples, as seen in the figure 6.3, reduces the noise slightly compared to the raw data version.

As we can see in the figure 6.4, adding the median on 3 samples to the mean does not improve the acquisition.
By adding a low pass filter at a frequency of 100 Hz as in the figure 6.5, it shows no differences compared to the version with only mean and median.
Frequency components above 100 Hz are probably not present.
In the paragraph on dynamic tests with datasets of a real shock absorber, the frequency study will be discussed to understand which frequencies are involved. The LPF can serve as a prevention for any high frequency noise which would be automatically filtered out.
From these static tests, the filter that leads to a notable improvement in the measurement is the mean. The raw signal is very noisy and the rolling-median and LPF have little impact on the measurement.

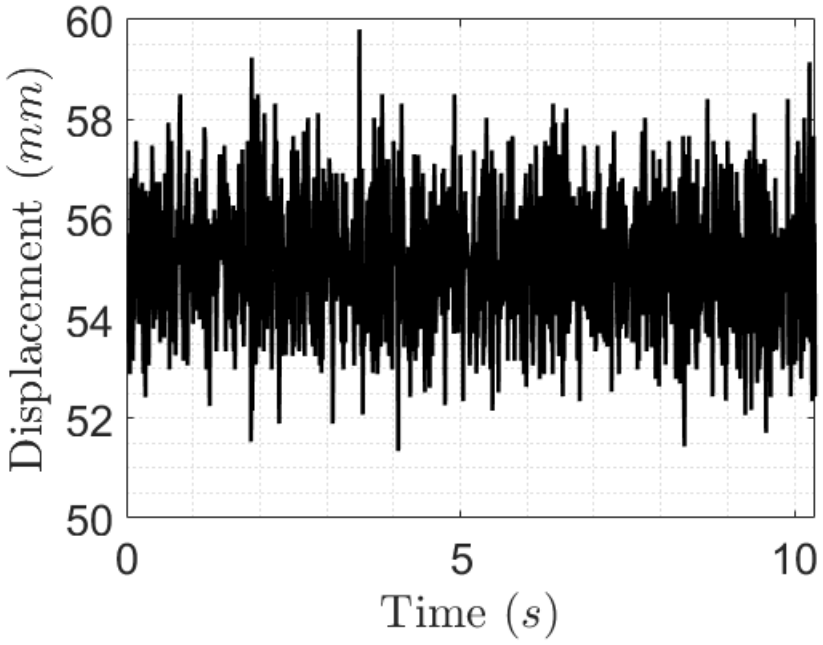

Figure 6.1. Static test of raw data.

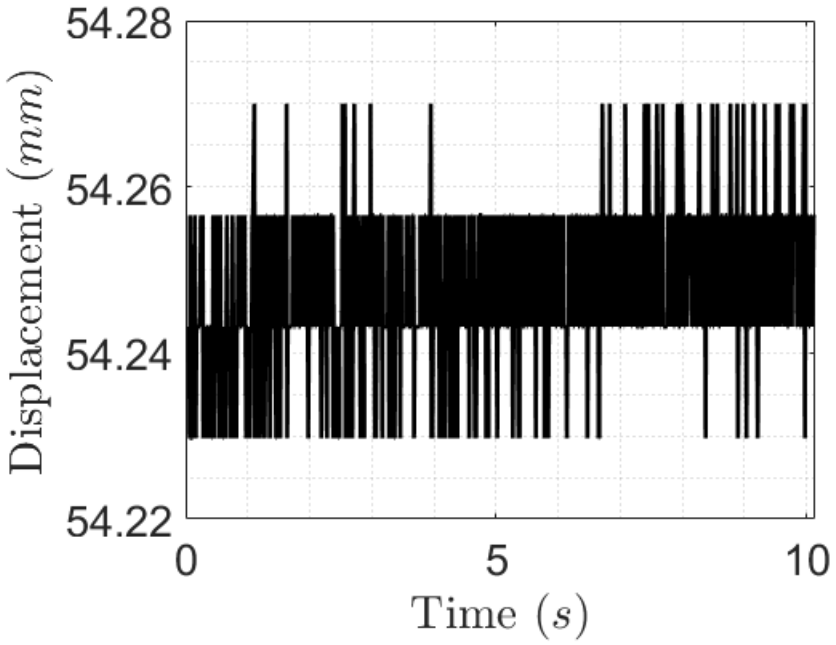

Figure 6.2. Static test with mean.

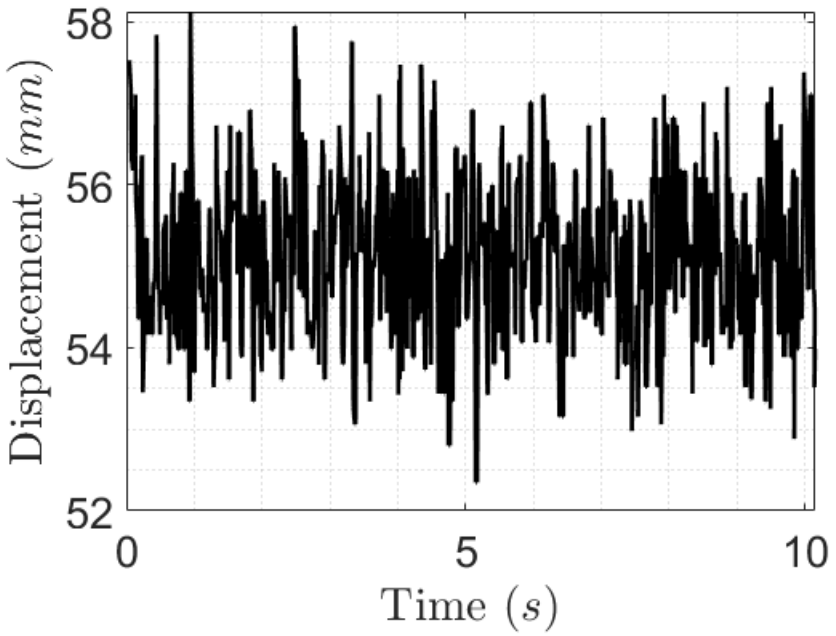

Figure 6.3. Static test with median on 3 samples.

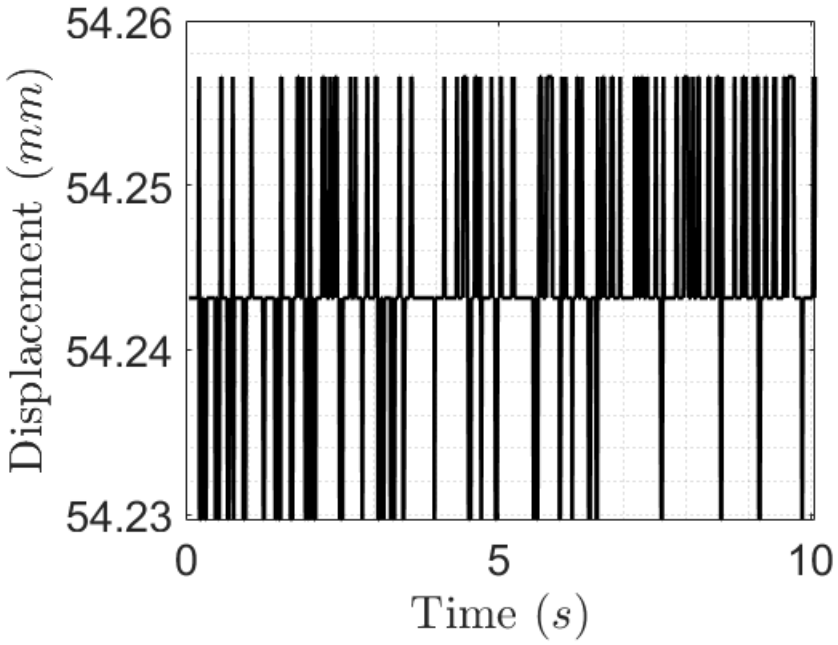

Figure 6.4. Static test with mean and median on 3 samples.

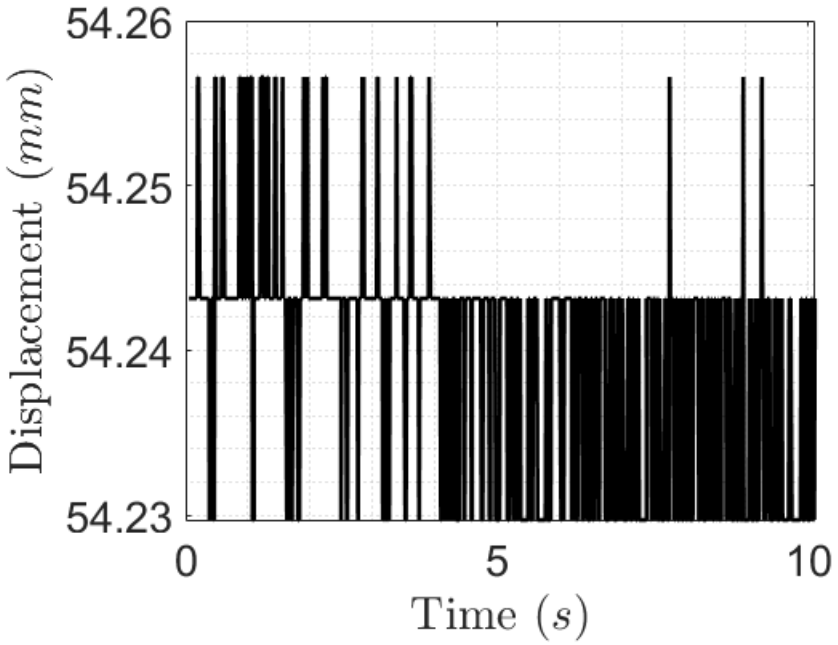

Figure 6.5. Static test with mean, median on 3 samples and LPF.

6.2 Dynamic tests

To simulate the displacement of the piston in the shock absorber, the variable capacitor moved by a servo motor was used as can be seen in the figure 6.6.
In this way we can program the servo by directly setting the PWM which corresponds to a precise angular position and consequently to a capacitance value.
The purpose of these dynamic tests is to understand if the sensor can keep up with the variation in the position of the shock absorber.
Analyzing the impact of the previously analyzed filters.

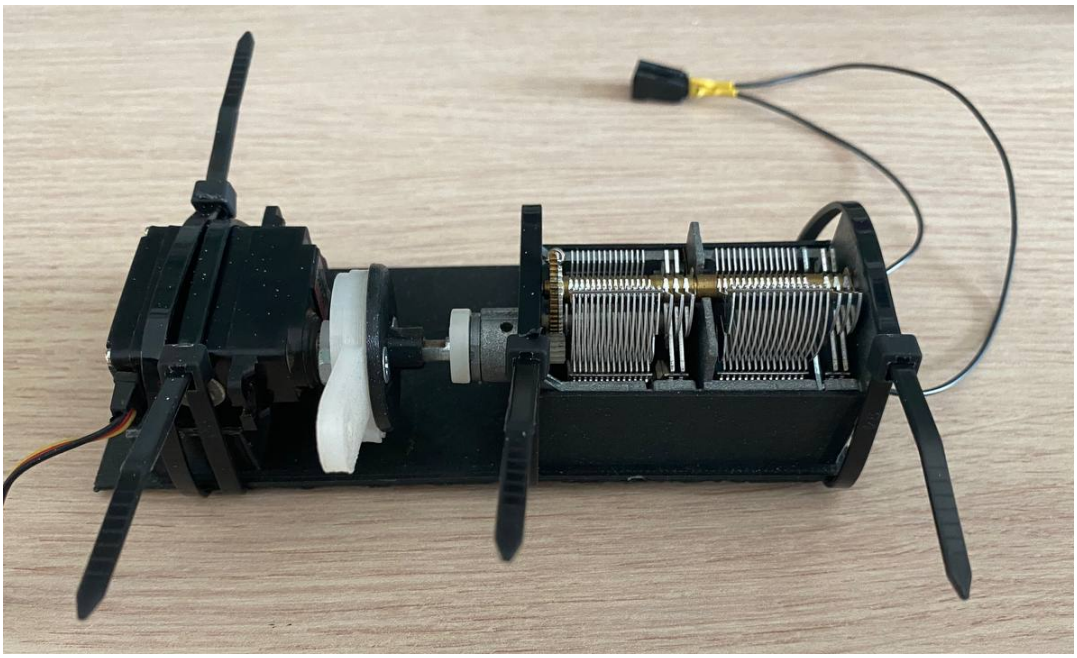

Figure 6.6. Servo motor and variable capacitor for dynamic tests.

6.2.1 Tests with linear displacement

For the first dynamic test the servo motor was set to copy a movement between -60 mm and 220 mm in 0.5 seconds.
The maximum slew rate is limited by the angular speed of the servo motor. For the test in question it is more than sufficient.
As we can see from the figure 6.7 without using any type of filter the signal is noisy only in the flat areas, during the movement it is quite linear.

With the use of the mean, figure 6.8, we notice a notable reduction in noise in the flat areas and an overshoot emerges, probably due to the position control of the servo motor, which we did not notice before.
The use of the 3-sample median is shown in the figure 6.9, even in this case there is no clear improvement in the characteristic.
The use of the mean and median as in the figure 6.10 and the addition of the low pass filter in the figure 6.11 do not show improvements compared to simply using the only mean.

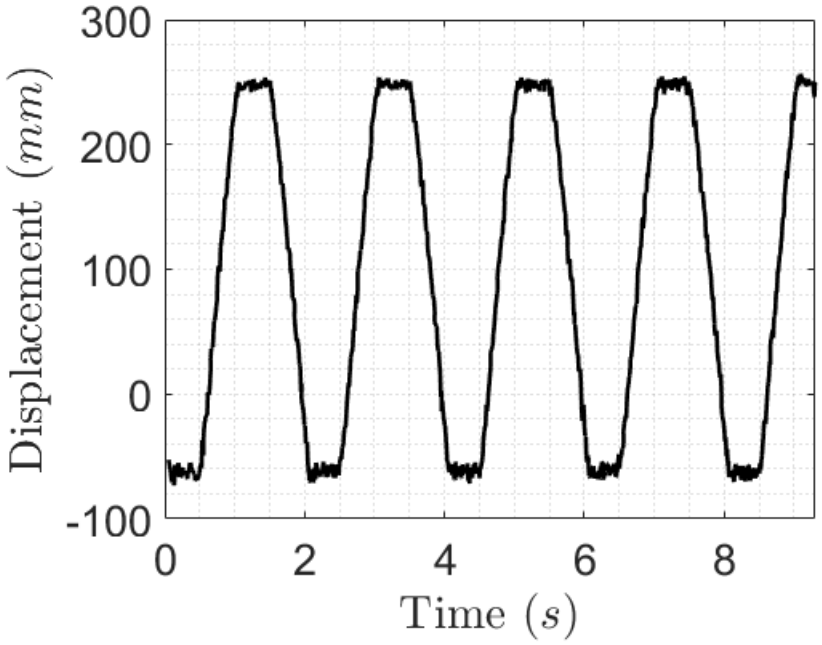

Figure 6.7. Linear dinamic test of raw data.

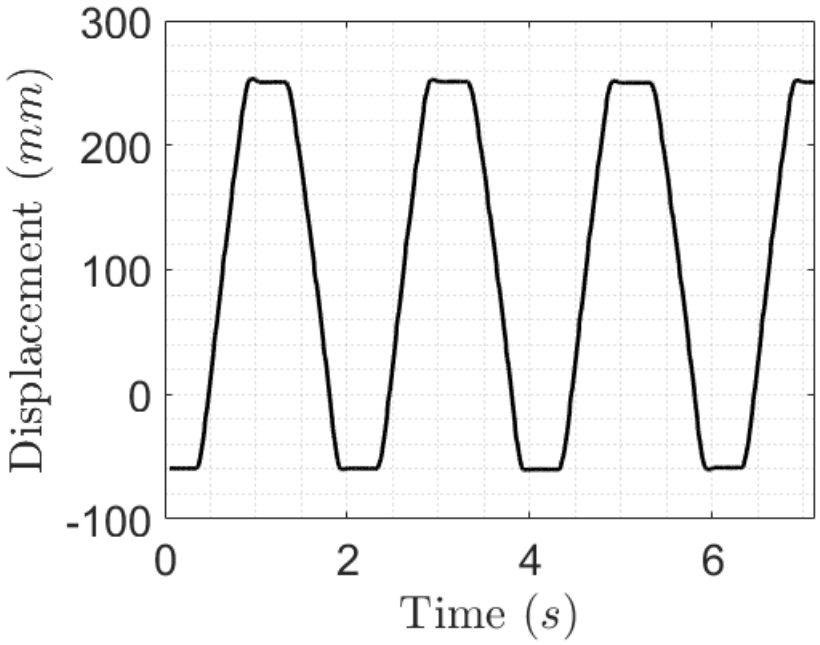

Figure 6.8. Linear dinamic test with mean.

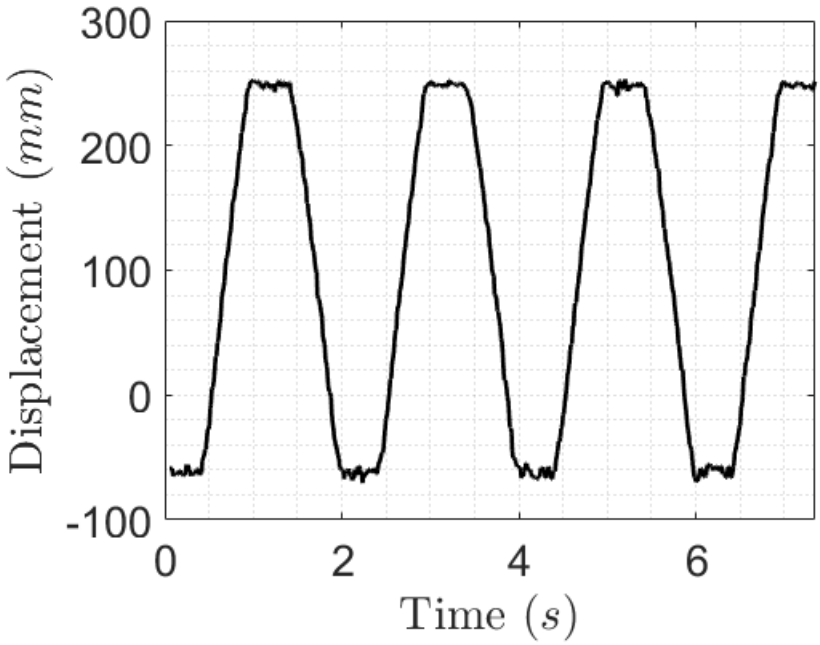

Figure 6.9. Linear dinamic test with median on 3 samples.

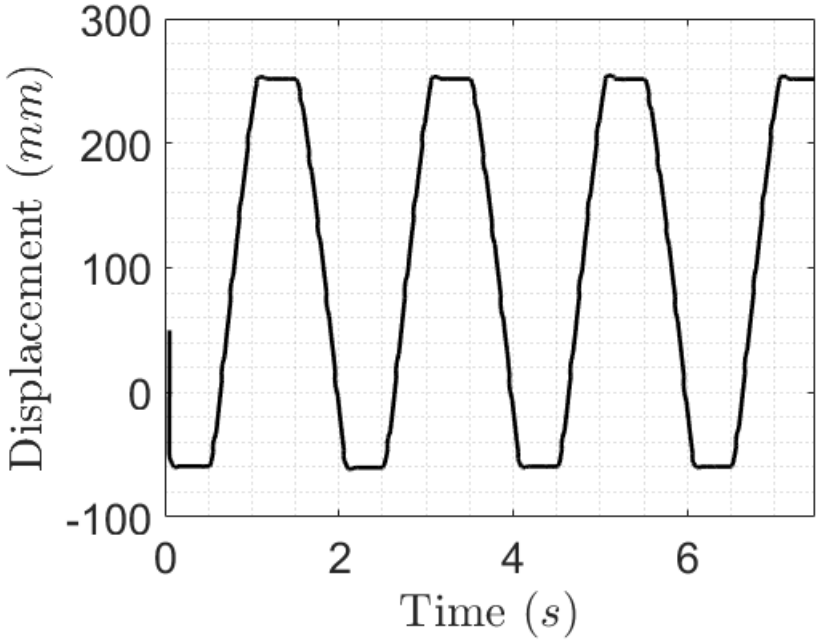

Figure 6.10. Linear dinamic test with mean and median on 3 samples.

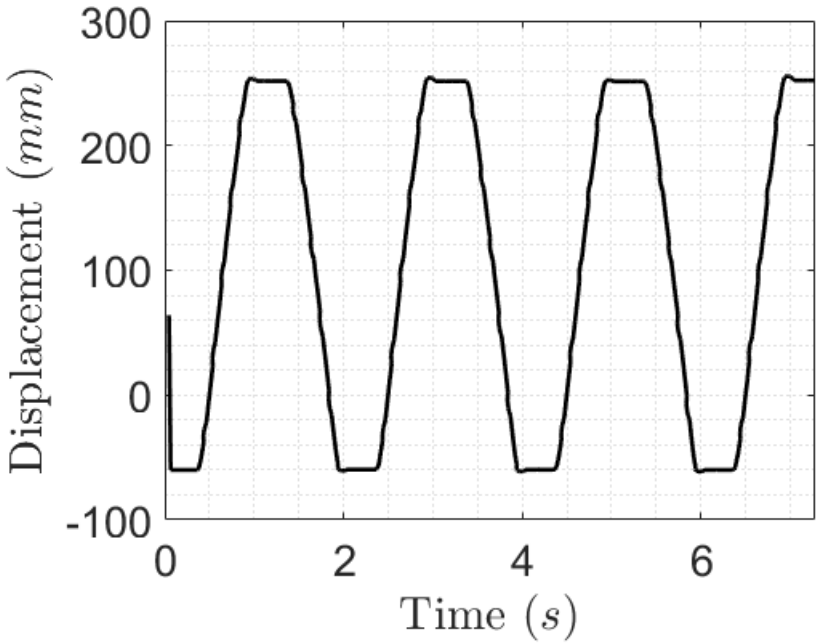

Figure 6.11. Linear dinamic test with mean, median on 3 samples and LPF.

6.2.2 Test with real dataset

To study the behavior of the various filters applied to the real movement of the shock absorber on the road we used two displacement datasets of a real shock absorber.
The displacement dataset was converted to angular position and later on given as a command to the servo motor.
Two different datasets were used in order to verify the behavior of the sensor dynamics. Below are the results of the measurements obtained.

Dataset 1

The first dataset has a dynamic that varies between -30 mm compared to the rest position of the shock absorber up to 0 mm.
The cycle in question has a duration of 25 seconds and as we can see from the figure 6.12 without the use of filters the signal measured by the sensor follows the peaks of the dataset very well but is very noisy. In particular, in the period between 10 seconds and 15 seconds in which we have a minimum relative displacement, it is not possible to distinguish the trend of the position of the shock absorber.
The problem is solved by using the mean, figure 6.13. Also in this case the displacement peaks are followed correctly, the signal is much less noisy and the position of the shock absorber can be followed well even in the "flat" points.
The use of the median on 3 samples, figure 6.14, reduces the noise compared to the test without filters but is still very noisy when compared with the mean.
By combining mean and median as in the figure 6.15 we do not obtain any improvement compared to the version with only the mean.
The reason could be due to the median made on 3 samples. In the next dataset the median will be tested on 10 samples and on 20 samples to verify whether the use of the rolling-median does not improve the measurement quality compared to the mean.
Finally, the low pass filter with a frequency of 100 Hz was applied and as we can see from the figure 6.16, the result is practically identical to the test using only the mean.

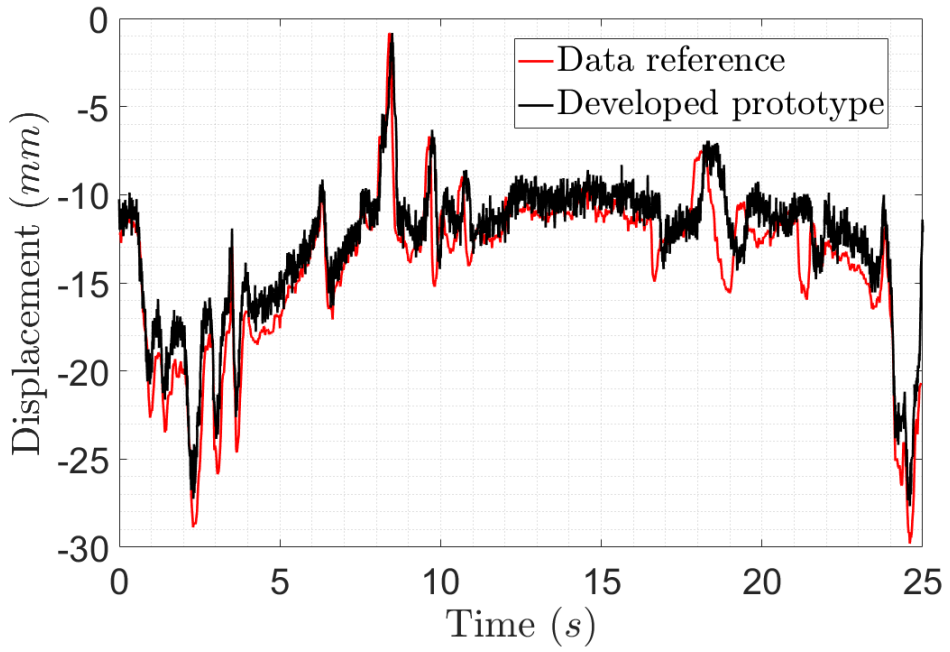

Figure 6.12. Comparison of dataset #1 and raw measurement of the prototype.

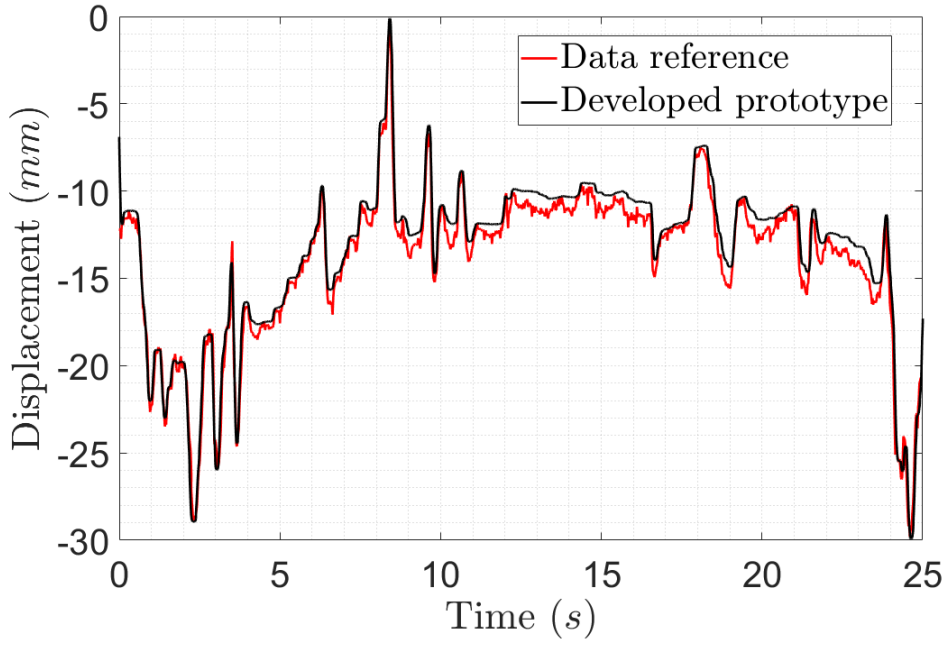

Figure 6.13. Comparison of dataset #1 and prototype measurement with mean.

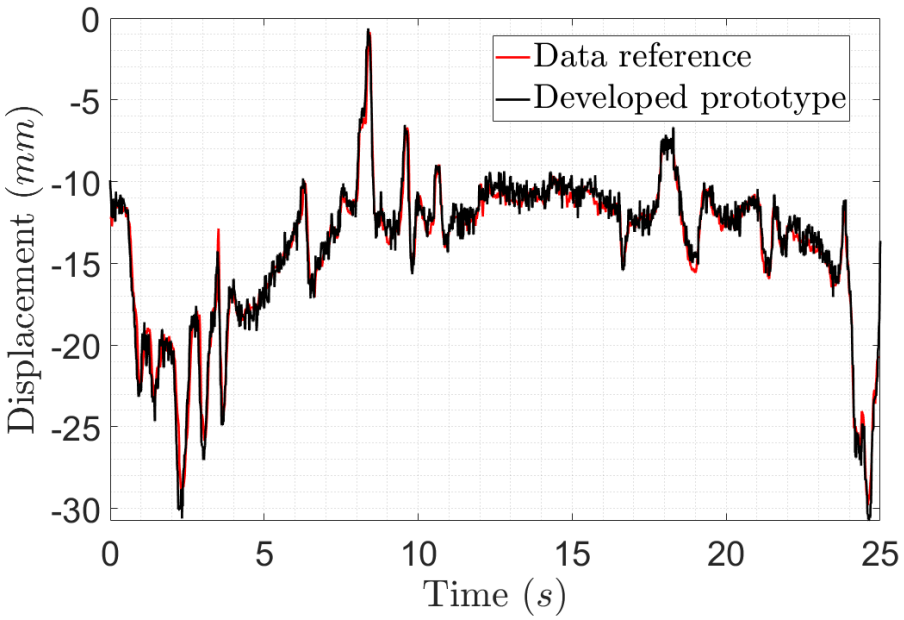

Figure 6.14. Comparison of dataset #1 and prototype measurement with median on 3 samples.

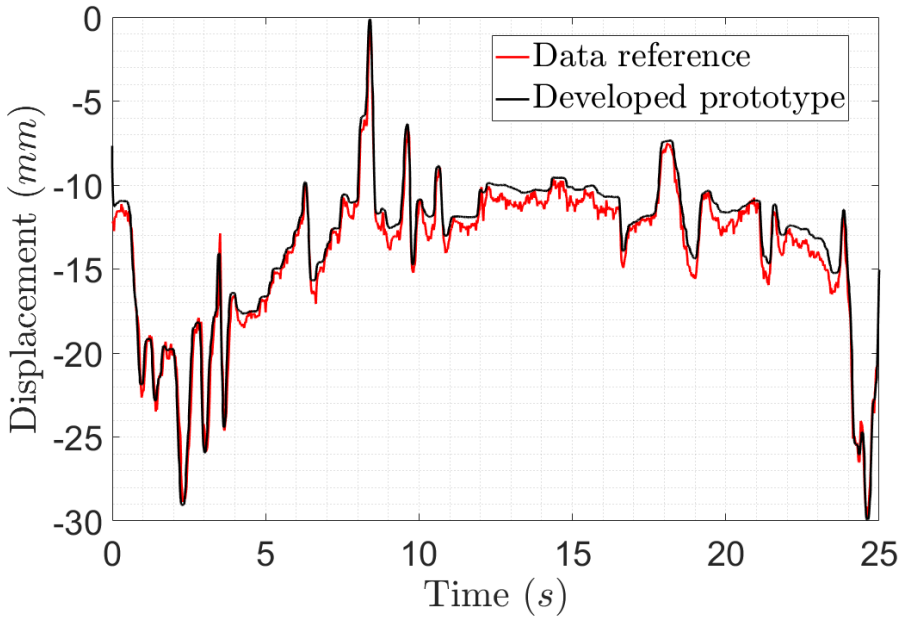

Figure 6.15. Comparison of dataset #1 and prototype measurement with mean and median on 3 samples.

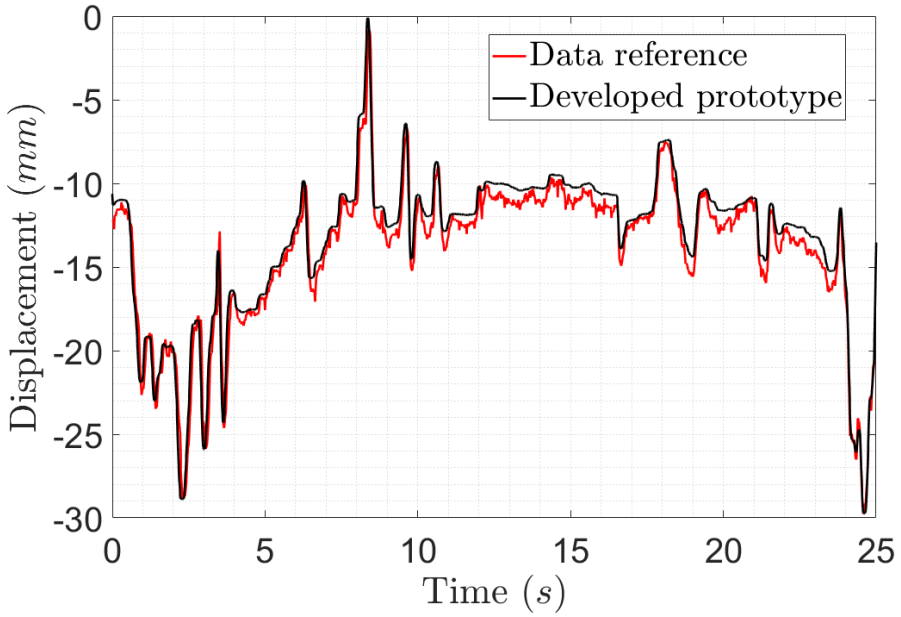

Figure 6.16. Comparison of dataset #1 and prototype measurement with mean, median on 3 samples and LPF.

Dataset 2

The second dataset used has similar dynamics to the previous one, approximately 30 mm of displacement between the piston and cylinder.
This dataset in particular has more spikes than the other.
As we can see, the sensor follows the trend of the reference very well although the spikes, we can therefore confirm that the sensor keep up with the dynamics of a shock absorber.
In this test, the 3-samples, 10-samples and 20-samples median was used to verify if the median is useful for improving the quality of the measurement.
The figure 6.17 shows the raw data without any type of filter, the signal is very noisy but still follows the trend well.
By using the mean, figure 6.18 the result is significantly improved, losing a bit of definition in the area between 5 seconds, where the measured signal appears to be in "flat" steps.
Even in this test the use of the 3-samples median does not improve the measurement, figure 6.19.
While the use of the 10-samples median improves the problem encountered with the mean figure 6.20. The signal seems to follow the reference better around 5 seconds. Using the median on 10 samples or 20 samples, as seen in the figure 6.21, instead worsens the precision on the spikes which are more attenuated compared to the version with the mean, increasing the error on the displacement .
Adding the mean to the median over 20 samples, as seen in 6.22 does not improve the problems found only on the median, rather it adds the problems found only on the mean.
Even in this test, adding the LPF filter shows no visible results figure 6.23.

We can therefore conclude that the use of the mean significantly improves the quality of the measurement, while the median of 10 samples or 20 samples improves the local dynamics but loses precision on the measurement at the extremes of the dynamics.
The combination of mean and median is not functional. It is better to choose one or the other based on your needs.
The low pass filter set with a cut-off frequency of 100 Hz did not show significant differences, in the next paragraph the FFT of the given signal will be discussed for analyzing the spectral components of the dataset.

6.2.3 FFT of the dataset

Finally, the FFT of a displacement profile of the shock absorber was calculated in order to see the spectral components that are involved.

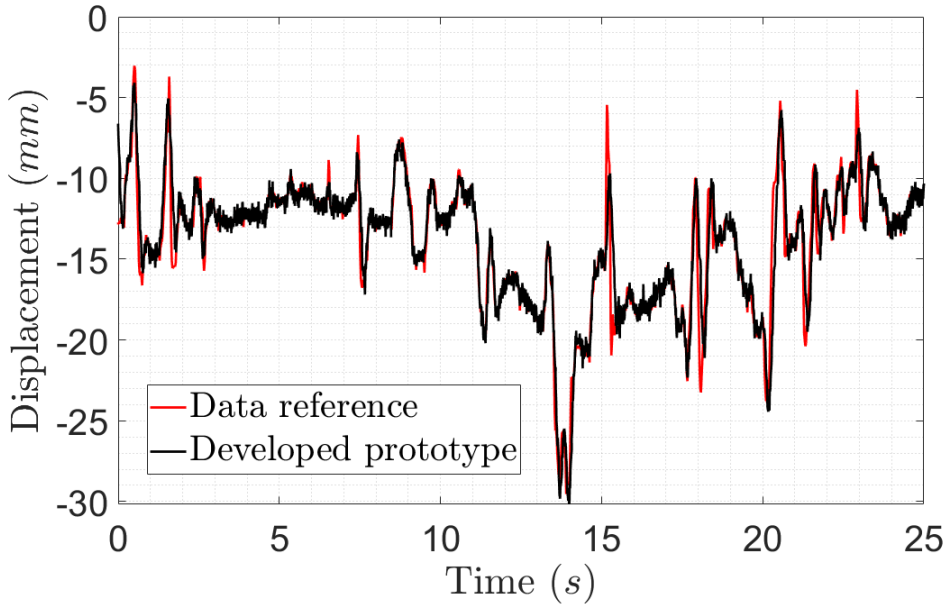

Figure 6.17. Comparison of dataset #2 and raw measurement of the prototype.

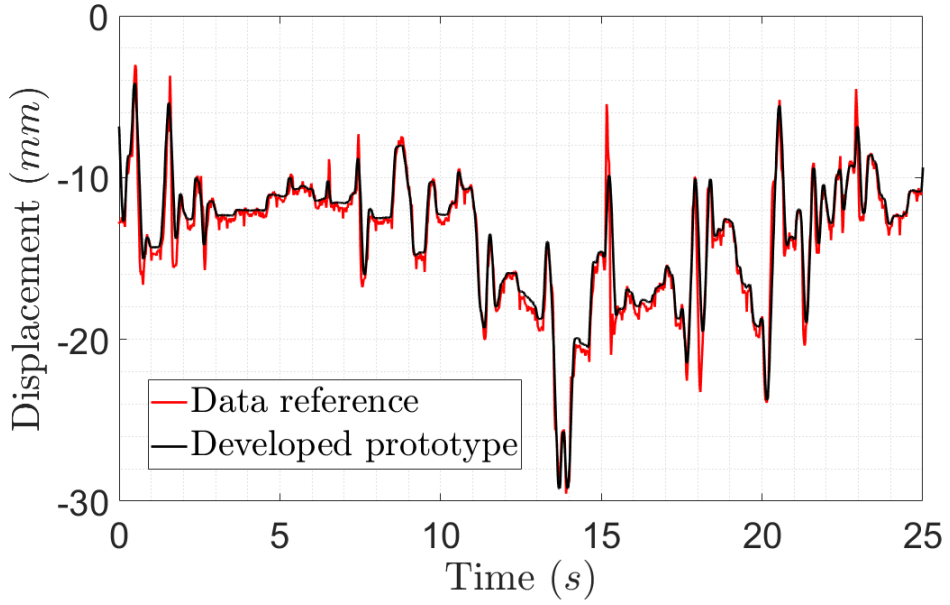

Figure 6.18. Comparison of dataset #2 and prototype measurement with mean.

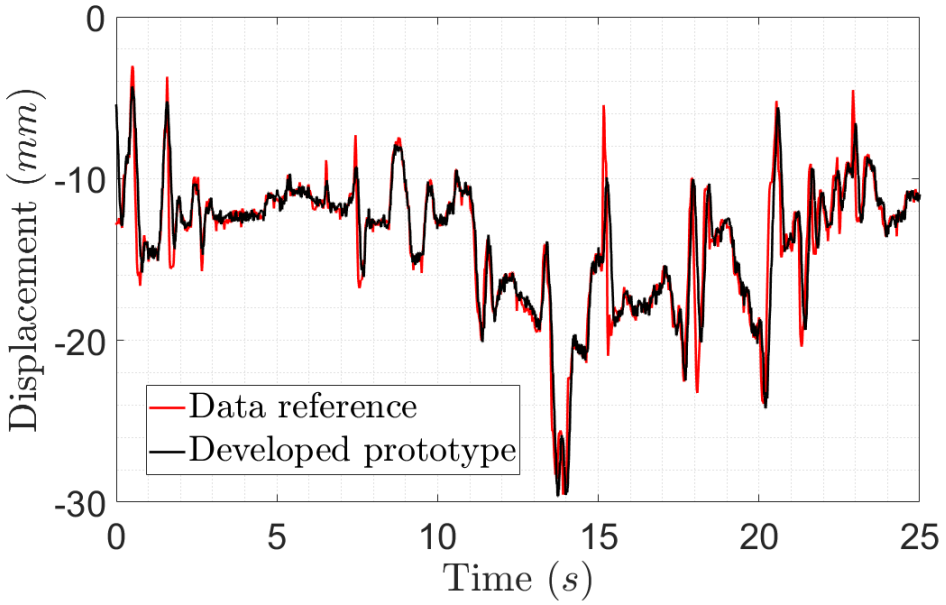

Figure 6.19. Comparison of dataset #2 and prototype measurement with median on 3 samples.

The FFT of the dataset is shown in figure 6.24 and as we can see the maximum frequency involved does not exceed 10 Hz.
The low pass filter previously set at 100 Hz is therefore not a problem for the dynamics of the shock absorber. It acts as a protection against any unwanted high frequency disturbances.
The FFT also confirms that the sampling frequency of 100 kHz is well above the minimum sampling frequency and allow us to rescaling, through the mean, the output frequency at 50 Hz to adapt the measurement to the CAN protocol.

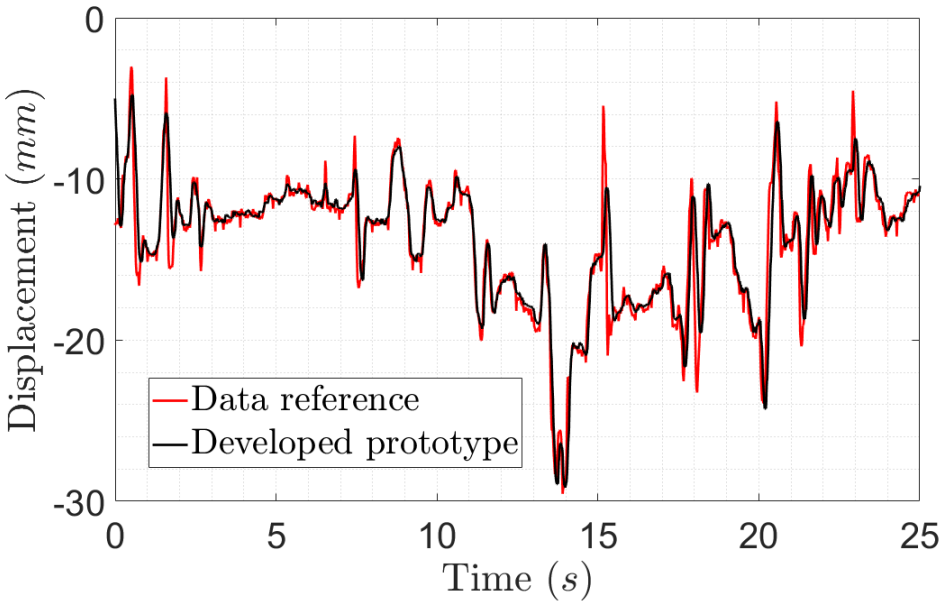

Figure 6.20. Comparison of dataset #2 and prototype measurement with median on 10 samples.

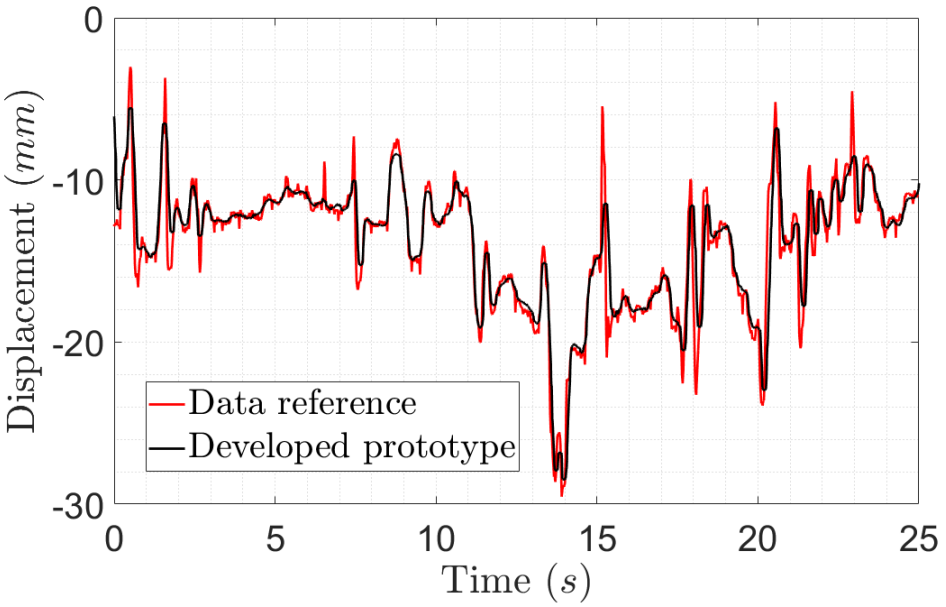

Figure 6.21. Comparison of dataset #2 and prototype measurement with median on 20 samples.

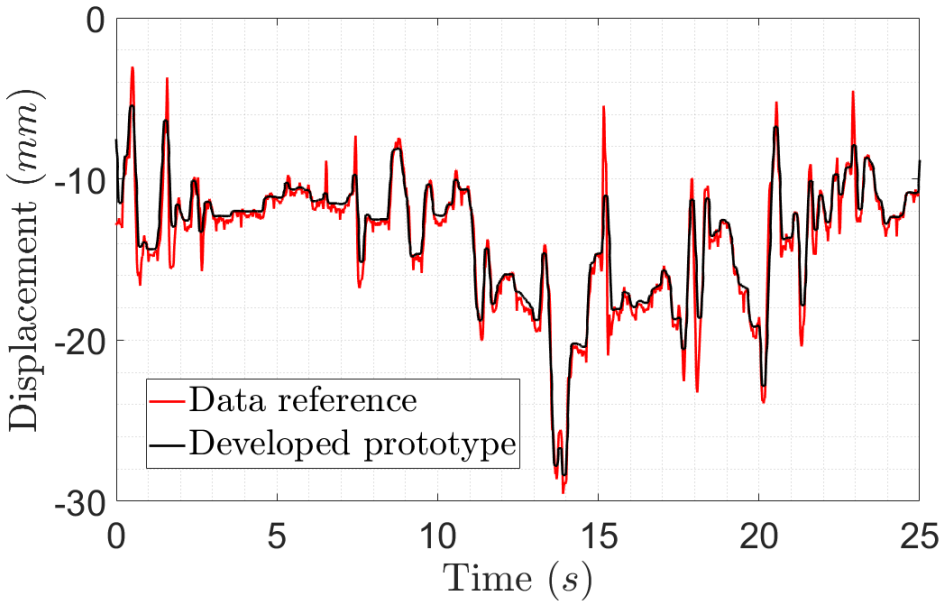

Figure 6.22. Comparison of dataset #2 and prototype measurement with mean and median on 20 samples.

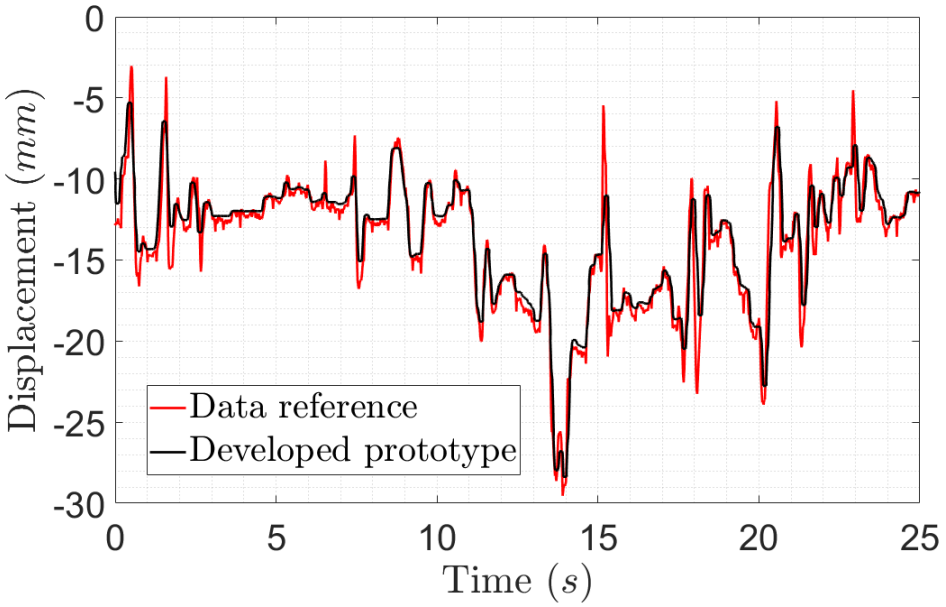

Figure 6.23. Comparison of dataset #2 and prototype measurement with mean, median on 20 samples and LPF.

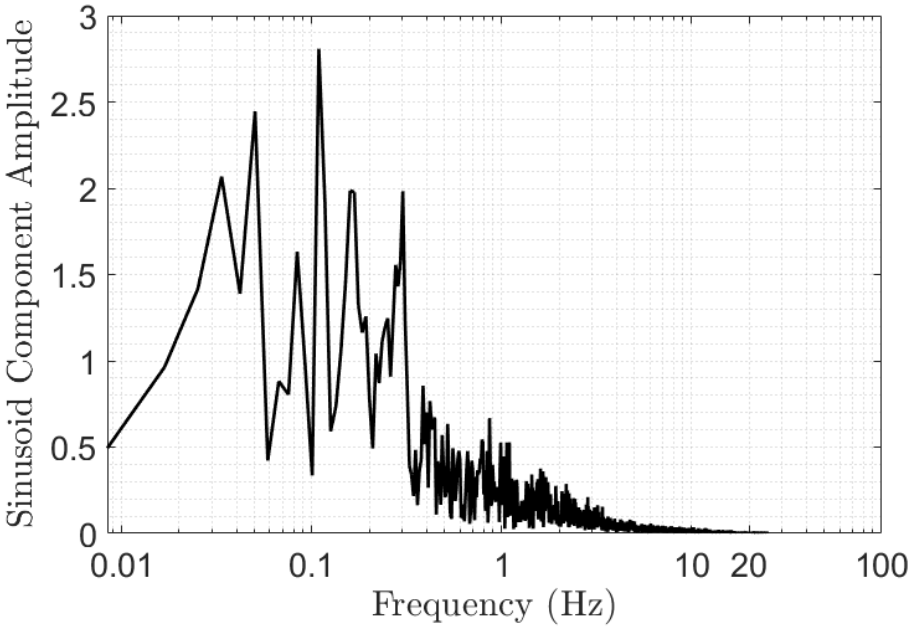

Figure 6.24. FFT of a dataset.

Chapter 7

Conclusion and future work

This new position sensor based on the measurement of shock absorber capacitance offers a new and innovative method of measuring the displacement between piston and cylinder in a non-intrusive manner and solving many of the problems present in position sensors currently used in the automotive field.
To reduce the measured position error, a calibration of the frequency-capacitance characteristic of the prototype was necessary.
During the tests, a difference in the capacitance reading over time of the same prototype was found, probably due to the temperature variation at which the tests were carried out.
Due to the tolerance of the prototype PCB components, a difference in reading was found between different prototypes.
This difference could also be caused by electromagnetic disturbances in the environment which have altered the capacitance value. Future analyses will be carried out to understand the reason for this difference and if it is due to the tolerance of the components, a solution could be a calibrate state to calibrating each PCB.
The variation in the dielectric constant of the shock absorber oil as the temperature varied was also analysed.
A test parallel plate capacitor was therefore built due to a simple geometry and later on immersed in synthetic oil in order to study the variation in capacitance and therefore dielectric constant.
The characteristic of variation of dielectric constant with temperature was used and implemented in the calculation of the position of the prototype.
Finally, the dynamic behavior of the sensor was analyzed with particular attention to the mean and median filters, analyzing their impact on the measurement precision.
Future work to move from a prototype phase to large-scale production is as follows.
Detailed analysis of the initial drift encountered during testing to understand what it

comes from and how to eliminate it.
Provide a calibration state in the microcontroller in which the capacitance of the shock absorber is measured in full compression and full extension in order to use the best characteristic depending on the PCB used.
This would resolve reading problems caused by PCB component tolerance.
Another future work is to determine the anchoring position of the sensor in the shock absorber. Depending on the position of the sensor, use controlled capacitance connection cables or integrate the sensor directly into the bolt in order to have access to the piston and cylinder without the use of connection cables.

This innovative position sensor can also be used in other fields such as robotics.
In industrial manipulators, rotary joints are mainly used whose position is given by awkward and bulky encoders.
It would be possible to add two metal plates to the joint in order to estimate its angular position by measuring the capacitance.
In a panorama of cobot industrial manipulators in which collaboration between robots and humans is always more necessary, collision detection is an increasingly important issue to allow the sharing of spaces between robots and humans.
Due to the fact that the electromagnetic field of the human body interferes with the measured capacitance, the sensor can be used as a position sensor by reducing the speed of the robot within a certain distance from the human and stopping it directly if a critical distance is exceeded.

Bibliography

A. J. Hayzen A. A. Carey. Dielectric constant and oil analysis. URL https://www.machinerylubrication.com/Read/226/dielectric-constant-oil-analysis#:~:text=The%20typical%20decrease%20in%20dielectric,oil%20molecules%20per%20unit%20volume.

ActiveSensors. URL https://www.activesensors.com/products.

Four-terminal. URL https://en.wikipedia.org/wiki/Four-terminal_sensing.

HellaSensor. URL https://www.hella.com/soe/en/Products/Product-detail-4957/?pid=2570.

Pierpaolo Sorbellini Giordano Greco Simone Marchetti Marco di Vittorio Piero Monchiero Marcello Chiaberge, Dario Gandini. Capacitive displacement sensor for a self-sensing shock-absorber piston-cylinder mechanism. *ICECCME 2023*, 19-21 July 2023.

Lawrence V. Hmurick Navarun Gupta, Sarosh Patel. Using an un-balanced ac wheatstone bridge to measure capacitance and inductance. *ComPE 2020*, 2-4 July 2020.

ShockAbsorber. URL https://en.wikipedia.org/wiki/Shock_absorber.

TLE2142. Tle214x, tle214xa excalibur low-noise high-speed precision operational amplifiers - texas instruments. URL https://www.ti.com/lit/ds/symlink/tle2142.pdf?ts=1612727624580&ref_url=https%253A%252F%252Fwww.ti.com%252Fproduct%252FTLE2142.